DPNU-05-09
TU-748

Resolution to the $B \to \pi K$ puzzle

Hsiang-nan Li[1],* Satoshi Mishima[2],† and A.I. Sanda[3]‡
[1] *Institute of Physics, Academia Sinica, Taipei, Taiwan 115, Republic of China*
[1] *Department of Physics, National Cheng-Kung University, Tainan, Taiwan 701, Republic of China*
[2] *Department of Physics, Tohoku University, Sendai 980-8578, Japan and*
[3] *Department of Physics, Nagoya University, Nagoya 464-8602, Japan*

We calculate the important next-to-leading-order contributions to the $B \to \pi K$, $\pi\pi$ decays from the vertex corrections, the quark loops, and the magnetic penguins in the perturbative QCD approach. It is found that the latter two reduce the leading-order penguin amplitudes by about 10%, and modify only the $B \to \pi K$ branching ratios. The main effect of the vertex corrections is to increase the small color-suppressed tree amplitude by a factor of 3, which then resolves the large difference between the direct CP asymmetries of the $B^0 \to \pi^\mp K^\pm$ and $B^\pm \to \pi^0 K^\pm$ modes. The puzzle from the large $B^0 \to \pi^0\pi^0$ branching ratio still remains.

PACS numbers: 13.25.Hw, 12.38.Bx, 11.10.Hi

I. INTRODUCTION

The B factories have accumulated enough events, which allow precision measurements of exclusive B meson decays. These measurements sharpen the discrepancies between experimental data and theoretical predictions within the standard model, such that some puzzles have appeared. The recently observed direct CP asymmetries and branching ratios of the $B \to \pi K$, $\pi\pi$ decays [1],

$$\begin{aligned} A_{CP}(B^0 \to \pi^\mp K^\pm) &= (-11.5 \pm 1.8)\% , \\ A_{CP}(B^\pm \to \pi^0 K^\pm) &= (4 \pm 4)\% , \\ B(B^0 \to \pi^+\pi^-) &= (5.0 \pm 0.4) \times 10^{-6} , \\ B(B^0 \to \pi^0\pi^0) &= (1.45 \pm 0.29) \times 10^{-6} , \end{aligned} \tag{1}$$

are prominent examples. The expected relations $A_{CP}(B^0 \to \pi^\mp K^\pm) \approx A_{CP}(B^\pm \to \pi^0 K^\pm)$ and $B(B^0 \to \pi^+\pi^-) \gg B(B^0 \to \pi^0\pi^0)$ obviously contradict to the above data. In this work we shall investigate the indication of Eq. (1), and study whether they can be accommodated in the perturbative QCD approach [2, 3].

To explain these puzzles, it is useful to adopt the topological-amplitude parameterization [4] for these decays. The most general parameterization of the $B \to \pi\pi$ decay amplitudes is written as

$$\begin{aligned} A(B^0 \to \pi^+\pi^-) &= -T\left(1 + \frac{P}{T}e^{i\phi_2}\right) , \\ \sqrt{2}A(B^+ \to \pi^+\pi^0) &= -T\left[1 + \frac{C}{T} + \frac{P_{ew}}{T}e^{i\phi_2}\right] , \\ \sqrt{2}A(B^0 \to \pi^0\pi^0) &= T\left[\left(\frac{P}{T} - \frac{P_{ew}}{T}\right)e^{i\phi_2} - \frac{C}{T}\right] , \end{aligned} \tag{2}$$

where T, C, P, and P_{ew} stand for the color-allowed tree, color-suppressed tree, penguin, and electroweak penguin amplitudes, respectively, and ϕ_2 is the weak phase defined later. The counting rules in terms of powers

*Electronic address: hnli@phys.sinica.edu.tw
†Electronic address: mishima@tuhep.phys.tohoku.ac.jp
‡Electronic address: sanda@eken.phys.nagoya-u.ac.jp

of the Wolfenstein parameter $\lambda \sim 0.22$ are then assigned to various decay amplitudes [5, 6, 7]. The amplitudes in Eq. (2) obey the counting rules in the standard model,

$$\frac{P}{T} \sim \lambda \,, \quad \frac{C}{T} \sim \lambda \,, \quad \frac{P_{ew}}{T} \sim \lambda^2 \,. \tag{3}$$

Therefore, the $B^0 \to \pi^0\pi^0$ branching ratio is expected to be of $O(\lambda^2)$ of the $B^0 \to \pi^+\pi^-$ one. However, Eq. (1) shows that the former is about of $O(\lambda)$ of the latter.

The $B \to \pi K$ decay amplitudes are written, up to $O(\lambda^2)$, as

$$\begin{aligned}
A(B^+ \to \pi^+ K^0) &= P' \,, \\
\sqrt{2}A(B^+ \to \pi^0 K^+) &= -P' \left[1 + \frac{P'_{ew}}{P'} + \left(\frac{T'}{P'} + \frac{C'}{P'} \right) e^{i\phi_3} \right] \,, \\
A(B^0 \to \pi^- K^+) &= -P' \left(1 + \frac{T'}{P'} e^{i\phi_3} \right) \,, \\
\sqrt{2}A(B^0 \to \pi^0 K^0) &= P' \left(1 - \frac{P'_{ew}}{P'} - \frac{C'}{P'} e^{i\phi_3} \right) \,,
\end{aligned} \tag{4}$$

where the notations T' C', P' and P'_{ew} bear the meanings the same as for the $B \to \pi\pi$ decays but with primes, and the weak phase ϕ_3 is defined via the Cabibbo-Kobayashi-Maskawa (CKM) matrix element $V_{ub} = |V_{ub}| \exp(-i\phi_3)$ [8]. These amplitudes obey the counting rules,

$$\frac{T'}{P'} \sim \lambda \,, \quad \frac{P'_{ew}}{P'} \sim \lambda \,, \quad \frac{C'}{P'} \sim \lambda^2 \,. \tag{5}$$

The data $A_{CP}(B^0 \to \pi^\mp K^\pm) \approx -11\%$ implies a sizable relative strong phase between T' and P', which verifies our prediction made years ago using the PQCD approach [2]. Since both P'_{ew} and C' are subdominant, the approximate equality for the direct CP asymmetries $A_{CP}(B^\pm \to \pi^0 K^\pm) \approx A_{CP}(B^0 \to \pi^\mp K^\pm)$ is expected, which is, however, in conflict with the data in Eq. (1) dramatically.

It is then natural to conjecture a large P'_{ew} [7, 9, 10, 11, 12], which signals a new physics effect, a large C' [13, 14, 15, 16], or both [17, 18] in the $B \to \pi K$ decays. The large C' proposal seems to be favored by a recent analysis of the $B \to \pi K$, $\pi\pi$ data based on the amplitude parameterization [13]. Note that the current PQCD predictions for the two-body nonleptonic B decays were derived from the leading-order (LO) formalism. While LO PQCD implies a negligible C', it is possible that this supposedly tiny amplitude may receive a significant subleading correction. Hence, before claiming a new physics signal, one should at least examine whether the next-to-leading-order (NLO) effects could enhance C' sufficiently. In this paper we shall calculate the important NLO contributions to the $B \to \pi K$, $\pi\pi$ decays from the vertex corrections, the quark loops, and the magnetic penguins. The higher-power corrections have not yet been under good control, and will not be considered here. We find that the corrections from the quark loops and from the magnetic penguins, being about 10% of the LO penguin amplitude, decrease only the $B \to \pi K$ branching ratios. The vertex corrections tend to increase C' by a factor of 3. This larger C' leads to nearly vanishing $A_{CP}(B^\pm \to \pi^0 K^\pm)$ without changing the branching ratios, which are governed by P'. The $B \to \pi K$ puzzle is then resolved.

The other NLO corrections, mainly to the B meson transition form factors, can be eliminated by choosing an appropriate renormalization scale $\mu \sim \sqrt{\bar{\Lambda} m_b}$, $\bar{\Lambda}$ being a hadronic scale and m_b the b quark mass. This observation follows the well-known Brodsky-Lepage-Mackenzie (BLM) procedure [19], in which the scale μ is determined in the way that the vacuum polarization effects are absorbed into the coupling constant $\alpha_s(\mu)$. It has been demonstrated with this procedure that NLO corrections to many exclusive processes are minimized to some extent [19]. Taking the simple pion form factor as an example, the BLM scale has been found to be of the order of the invariant mass of the hard exchanged gluon. The choice of μ proposed in the PQCD approach [20] is basically in agreement with this procedure: the argument μ of the coupling constant is set to the invariant masses of internal particles, which are of $O(\sqrt{\bar{\Lambda} m_b})$ for the B meson transition form factors [21, 22, 23]. A general feature of the BLM scale is that it is always much lower than the external kinematic variable, implying that the smallness of the coupling constant is not the only condition for the applicability of perturbation theory.

As mentioned before, the observed branching ratio $B(B^0 \to \pi^0\pi^0) \approx 1.5 \times 10^{-6}$ is much larger than the LO PQCD prediction $\sim 10^{-7}$ [3, 24]. The prediction from QCD-improved factorization (QCDF) has the same order

of magnitude [25]. Since this mode involves a subdominant color-suppressed tree amplitude as shown in Eq. (2), a larger C certainly helps to resolve the $B \to \pi\pi$ puzzle. We also compute the NLO corrections to these decays, and find the similar reduction from the quark loops and the magnetic penguins, which are about 10% of the LO penguin amplitude P. Since P is subdominant, the $B^0 \to \pi^\mp\pi^\pm$ and $B^\pm \to \pi^\pm\pi^0$ branching ratios almost remain the same. The enhancement of C from the vertex corrections, leading to $B(B^0 \to \pi^0\pi^0) \approx 0.3 \times 10^{-6}$, is still not sufficient to account for the data. We point out that any new mechanism, introduced to resolve this puzzle, must survive the constraint from the tiny observed branching ratios [1],

$$\begin{aligned} B(B^0 \to K^0\overline{K}^0) &= (0.96^{+0.25}_{-0.24}) \times 10^{-6} , \\ B(B^0 \to \rho^0\rho^0) &< 1.1 \times 10^{-6} . \end{aligned} \tag{6}$$

The leading PQCD predictions for $B(B^0 \to K^0\overline{K}^0)$ [26] and for $B(B^0 \to \rho^0\rho^0)$ [27, 28] have been consistent with the experimental data. The proposals of final-state interaction [29] and of the charming penguin in soft-collinear effective theory (SCET) [30] have not yet been applied to the $B^0 \to \rho^0\rho^0$ decay.

We review the LO PQCD predictions for the $B \to \pi K$, $\pi\pi$ decays, including those for the mixing-induced CP asymmetries, in Sec. II. The vertex corrections, the quark loops, and the magnetic penguin amplitudes are computed in Sec. III. We perform the numerical study in Sec. IV, where the theoretical uncertainty is also analyzed. Section V is the conclusion. The explicit factorization formulas for the various topologies of decay amplitudes are collected in Appendix.

II. LEADING-ORDER PREDICTIONS

The effective Hamiltonian for the $b \to s$ transition is given by [31],

$$H_{\rm eff} = \frac{G_F}{\sqrt{2}} \sum_{q=u,c} V_{qb}V_{qs}^* \left[C_1(\mu)O_1^{(q)}(\mu) + C_2(\mu)O_2^{(q)}(\mu) + \sum_{i=3}^{10} C_i(\mu)O_i(\mu) \right] , \tag{7}$$

with the Fermi constant $G_F = 1.16639 \times 10^{-5}$ GeV^{-2}, and the CKM matrix elements V. The four-fermion operators are written as

$$\begin{aligned} O_1^{(q)} &= (\bar{s}_i q_j)_{V-A}(\bar{q}_j b_i)_{V-A} , & O_2^{(q)} &= (\bar{s}_i q_i)_{V-A}(\bar{q}_j b_j)_{V-A} , \\ O_3 &= (\bar{s}_i b_i)_{V-A} \sum_{q'} (\bar{q}'_j q'_j)_{V-A} , & O_4 &= (\bar{s}_i b_j)_{V-A} \sum_{q'} (\bar{q}'_j q'_i)_{V-A} , \\ O_5 &= (\bar{s}_i b_i)_{V-A} \sum_{q'} (\bar{q}'_j q'_j)_{V+A} , & O_6 &= (\bar{s}_i b_j)_{V-A} \sum_{q'} (\bar{q}'_j q'_i)_{V+A} , \\ O_7 &= \frac{3}{2}(\bar{s}_i b_i)_{V-A} \sum_{q'} e_{q'} (\bar{q}'_j q'_j)_{V+A} , & O_8 &= \frac{3}{2}(\bar{s}_i b_j)_{V-A} \sum_{q'} e_{q'} (\bar{q}'_j q'_i)_{V+A} , \\ O_9 &= \frac{3}{2}(\bar{s}_i b_i)_{V-A} \sum_{q'} e_{q'} (\bar{q}'_j q'_j)_{V-A} , & O_{10} &= \frac{3}{2}(\bar{s}_i b_j)_{V-A} \sum_{q'} e_{q'} (\bar{q}'_j q'_i)_{V-A} , \end{aligned} \tag{8}$$

with the color indices i, j, and the notations $(\bar{q}'q')_{V\pm A} = \bar{q}'\gamma_\mu(1 \pm \gamma_5)q'$. The index q' in the summation of the above operators runs through u, d, s, c, and b. The effective Hamiltonian for the $b \to d$ transition is obtained by changing s into d in Eqs. (7) and (8).

According to Eq. (7), the amplitude for a B meson decay into the final state f through the $\bar{b} \to \bar{s}(\bar{d})$ transition has the general expression,

$$\mathcal{A}(B \to f) = V_{ub}^* V_{us(d)}\, \mathcal{A}_f^{(u)} + V_{cb}^* V_{cs(d)}\, \mathcal{A}_f^{(c)} + V_{tb}^* V_{ts(d)}\, \mathcal{A}_f^{(t)} . \tag{9}$$

For $f = \pi K$, the amplitudes $\mathcal{A}_{\pi K}^{(u)}$, $\mathcal{A}_{\pi K}^{(c)}$, and $\mathcal{A}_{\pi K}^{(t)}$ are decomposed at LO into

$$\begin{aligned} \mathcal{A}_{\pi K}^{(u)} &= f_K F_e + \mathcal{M}_e + f_\pi F_{eK} + \mathcal{M}_{eK} + f_B F_a + \mathcal{M}_a , \\ \mathcal{A}_{\pi K}^{(c)} &= 0 , \\ \mathcal{A}_{\pi K}^{(t)} &= -\left(f_K F_e^P + \mathcal{M}_e^P + f_\pi F_{eK}^P + \mathcal{M}_{eK}^P + f_B F_a^P + \mathcal{M}_a^P \right) , \end{aligned} \tag{10}$$

where f_B (f_K, f_π) is the B meson (kaon, pion) decay constant, F_e ($\mathcal{M}_e$) the color-allowed factorizable (nonfactorizable) tree emission contribution, F_{eK} ($\mathcal{M}_{eK}$) the color-suppressed factorizable (nonfactorizable) tree emission contribution, F_a ($\mathcal{M}_a$) the factorizable (nonfactorizable) tree annihilation contribution, and those with the additional superscripts P the contributions from the penguin operators. For $f = \pi\pi$, the amplitudes $\mathcal{A}^{(u)}_{\pi\pi}$, $\mathcal{A}^{(c)}_{\pi\pi}$, and $\mathcal{A}^{(t)}_{\pi\pi}$ are decomposed at LO into

$$\begin{aligned}
\mathcal{A}^{(u)}_{\pi\pi} &= f_\pi F_e + \mathcal{M}_e + f_B F_a + \mathcal{M}_a \,, \\
\mathcal{A}^{(c)}_{\pi\pi} &= 0 \,, \\
\mathcal{A}^{(t)}_{\pi\pi} &= -\left(f_\pi F^P_e + \mathcal{M}^P_e + f_B F^P_a + \mathcal{M}^P_a\right) \,,
\end{aligned} \tag{11}$$

where we do not distinguish the color-allowed and color-suppressed contributions.

The factorization formulas for the various contributions to each $B \to \pi K$, $\pi\pi$ mode are collected in Tables I and II, and in Appendix, whose dependence on the Wilson coefficients has been made explicit. We define the standard combinations,

$$\begin{aligned}
a_1(\mu) &= C_2(\mu) + \frac{C_1(\mu)}{N_c} \,, \\
a_2(\mu) &= C_1(\mu) + \frac{C_2(\mu)}{N_c} \,, \\
a_i(\mu) &= C_i(\mu) + \frac{C_{i\pm1}(\mu)}{N_c} \,, \quad i = 3 \sim 10 \,,
\end{aligned} \tag{12}$$

where the upper (lower) sign applies, when i is odd (even). The coefficients a and a' in Tables I and II, besides a_1 and a_2 given above, are then written as

$$\begin{aligned}
a'_1 &= C_1 \,, & a'_2 &= C_2 \,, \\
a^{(q')}_3 &= a_3 + \frac{3}{2} e_{q'} a_9 \,, & a^{\prime(q')}_3 &= C_4 + \frac{3}{2} e_{q'} C_{10} \,, \\
a^{(q')}_4 &= a_4 + \frac{3}{2} e_{q'} a_{10} \,, & a^{\prime(q')}_4 &= C_3 + \frac{3}{2} e_{q'} C_9 \,, \\
a^{(q')}_5 &= a_5 + \frac{3}{2} e_{q'} a_7 \,, & a^{\prime(q')}_5 &= C_6 + \frac{3}{2} e_{q'} C_8 \,, \\
a^{(q')}_6 &= a_6 + \frac{3}{2} e_{q'} a_8 \,, & a^{\prime(q')}_6 &= C_5 + \frac{3}{2} e_{q'} C_7 \,.
\end{aligned} \tag{13}$$

With the amplitude $\mathcal{A}(B \to f)$ being computed using Eq. (9), we derive the two-body nonleptonic B meson decay rates and CP asymmetries. The former are given by

$$\Gamma(B \to f) = \frac{G_F^2 m_B^3}{128\pi} |\mathcal{A}(B \to f)|^2 \,, \tag{14}$$

where m_B is the B meson mass. The time-dependent CP asymmetry of the $B^0 \to \pi^0 K_S$ mode is defined as

$$\begin{aligned}
A_{CP}(B^0(t) \to \pi^0 K_S) &\equiv \frac{B(\bar{B}^0(t) \to \pi^0 K_S) - B(B^0(t) \to \pi^0 K_S)}{B(\bar{B}^0(t) \to \pi^0 K_S) + B(B^0(t) \to \pi^0 K_S)} \\
&= A_{\pi^0 K_S} \cos(\Delta M_d\, t) + S_{\pi^0 K_S} \sin(\Delta M_d\, t) \,,
\end{aligned} \tag{15}$$

with the mass difference ΔM_d of the two B-meson mass eigenstates, and the direct asymmetry and the mixing-induced asymmetry,

$$A_{\pi^0 K_S} = \frac{|\lambda_{\pi^0 K_S}|^2 - 1}{1 + |\lambda_{\pi^0 K_S}|^2} \,, \qquad S_{\pi^0 K_S} = \frac{2\,\mathrm{Im}(\lambda_{\pi^0 K_S})}{1 + |\lambda_{\pi^0 K_S}|^2} \,, \tag{16}$$

respectively. The $B^0 \to \pi^0 K_S$ decay has a CP-odd final state, and the corresponding factor,

$$\lambda_{\pi^0 K_S} = -e^{-2i\phi_1} \frac{P' - P'_{ew} - C' e^{-i\phi_3}}{P' - P'_{ew} - C' e^{i\phi_3}} \,, \tag{17}$$

where the weak phase ϕ_1 is defined via $V_{td} = |V_{td}|\exp(-i\phi_1)$. The time-dependent CP asymmetry of the $B^0 \to \pi^+\pi^-$ mode is defined by

$$\begin{aligned} A_{CP}(B^0(t) \to \pi^+\pi^-) &\equiv \frac{B(\bar{B}^0(t) \to \pi^+\pi^-) - B(B^0(t) \to \pi^+\pi^-)}{B(\bar{B}^0(t) \to \pi^+\pi^-) + B(B^0(t) \to \pi^+\pi^-)} \\ &= A_{\pi\pi}\cos(\Delta M_d\, t) + S_{\pi\pi}\sin(\Delta M_d\, t)\,, \end{aligned} \tag{18}$$

with the direct asymmetry and the mixing-induced asymmetry,

$$A_{\pi\pi} = \frac{|\lambda_{\pi\pi}|^2 - 1}{1 + |\lambda_{\pi\pi}|^2}\,, \qquad S_{\pi\pi} = \frac{2\,\mathrm{Im}(\lambda_{\pi\pi})}{1 + |\lambda_{\pi\pi}|^2}\,, \tag{19}$$

respectively, and the factor,

$$\lambda_{\pi\pi} = e^{2i\phi_2}\frac{T + Pe^{-i\phi_2}}{T + Pe^{i\phi_2}}\,, \tag{20}$$

	$\mathcal{A}^{(u)}_{\pi^+K^0}$	$\sqrt{2}\mathcal{A}^{(u)}_{\pi^0K^+}$
F_e	0	$F_{e4}\,(a_1)$
$\mathcal{M}_e$	0	$\mathcal{M}_{e4}\,(a_1')$
F_{eK}	0	$F_{eK4}\,(a_2)$
$\mathcal{M}_{eK}$	0	$\mathcal{M}_{eK4}\,(a_2')$
F_a	$F_{a4}\,(a_1)$	$F_{a4}\,(a_1)$
$\mathcal{M}_a$	$\mathcal{M}_{a4}\,(a_1')$	$\mathcal{M}_{a4}\,(a_1')$
	$\mathcal{A}^{(t)}_{\pi^+K^0}$	$\sqrt{2}\mathcal{A}^{(t)}_{\pi^0K^+}$
F_e^P	$F_{e4}\left(a_4^{(d)}\right) + F_{e6}\left(a_6^{(d)}\right)$	$F_{e4}\left(a_4^{(u)}\right) + F_{e6}\left(a_6^{(u)}\right)$
$\mathcal{M}_e^P$	$\mathcal{M}_{e4}\left(a_4^{\prime(d)}\right) + \mathcal{M}_{e6}\left(a_6^{\prime(d)}\right)$	$\mathcal{M}_{e4}\left(a_4^{\prime(u)}\right) + \mathcal{M}_{e6}\left(a_6^{\prime(u)}\right)$
F_{eK}^P	0	$F_{eK4}\left(a_3^{(u)} - a_3^{(d)} - a_5^{(u)} + a_5^{(d)}\right)$
$\mathcal{M}_{eK}^P$	0	$\mathcal{M}_{eK4}\left(a_3^{\prime(u)} - a_3^{\prime(d)} + a_5^{\prime(u)} - a_5^{\prime(d)}\right)$
F_a^P	$F_{a4}\left(a_4^{(u)}\right) + F_{a6}\left(a_6^{(u)}\right)$	$F_{a4}\left(a_4^{(u)}\right) + F_{a6}\left(a_6^{(u)}\right)$
$\mathcal{M}_a^P$	$\mathcal{M}_{a4}\left(a_4^{\prime(u)}\right) + \mathcal{M}_{a6}\left(a_6^{\prime(u)}\right)$	$\mathcal{M}_{a4}\left(a_4^{\prime(u)}\right) + \mathcal{M}_{a6}\left(a_6^{\prime(u)}\right)$
	$\mathcal{A}^{(u)}_{\pi^-K^+}$	$\sqrt{2}\mathcal{A}^{(u)}_{\pi^0K^0}$
F_e	$F_{e4}\,(a_1)$	0
$\mathcal{M}_e$	$\mathcal{M}_{e4}\,(a_1')$	0
F_{eK}	0	$F_{eK4}\,(a_2)$
$\mathcal{M}_{eK}$	0	$\mathcal{M}_{eK4}\,(a_2')$
F_a	0	0
$\mathcal{M}_a$	0	0
	$\mathcal{A}^{(t)}_{\pi^-K^+}$	$\sqrt{2}\mathcal{A}^{(t)}_{\pi^0K^0}$
F_e^P	$F_{e4}\left(a_4^{(u)}\right) + F_{e6}\left(a_6^{(u)}\right)$	$F_{e4}\left(-a_4^{(d)}\right) + F_{e6}\left(-a_6^{(d)}\right)$
$\mathcal{M}_e^P$	$\mathcal{M}_{e4}\left(a_4^{\prime(u)}\right) + \mathcal{M}_{e6}\left(a_6^{\prime(u)}\right)$	$\mathcal{M}_{e4}\left(-a_4^{\prime(d)}\right) + \mathcal{M}_{e6}\left(-a_6^{\prime(d)}\right)$
F_{eK}^P	0	$F_{eK4}\left(a_3^{(u)} - a_3^{(d)} - a_5^{(u)} + a_5^{(d)}\right)$
$\mathcal{M}_{eK}^P$	0	$\mathcal{M}_{eK4}\left(a_3^{\prime(u)} - a_3^{\prime(d)} + a_5^{\prime(u)} - a_5^{\prime(d)}\right)$
F_a^P	$F_{a4}\left(a_4^{(d)}\right) + F_{a6}\left(a_6^{(d)}\right)$	$F_{a4}\left(-a_4^{(d)}\right) + F_{a6}\left(-a_6^{(d)}\right)$
$\mathcal{M}_a^P$	$\mathcal{M}_{a4}\left(a_4^{\prime(d)}\right) + \mathcal{M}_{a6}\left(a_6^{\prime(d)}\right)$	$\mathcal{M}_{a4}\left(-a_4^{\prime(d)}\right) + \mathcal{M}_{a6}\left(-a_6^{\prime(d)}\right)$

TABLE I: $B \to \pi K$ decay amplitudes, whose factorization formulas are presented in Appendix.

where the weak phase ϕ_2 comes from the identity $\phi_2 = 180^\circ - \phi_1 - \phi_3$. In addition, the direct CP asymmetry for a charged B meson decay $B^+ \to f(B^- \to \bar{f})$ is defined by

$$A_{CP} = \frac{B(B^- \to \bar{f}) - B(B^+ \to f)}{B(B^- \to \bar{f}) + B(B^+ \to f)} \,. \tag{21}$$

The PQCD predictions for the branching ratios and the CP asymmetries of the $B \to \pi K$, $\pi\pi$ decays in the NDR scheme are listed in Tables III-VI. Using the LO and NLO Wilson coefficients, we obtain the values in the columns labelled by LO and $\mathrm{LO_{NLOWC}}$, respectively. It is noticed that some of the NLO Wilson coefficients, like C_5, diverge at a low scale. To derive the above tables, we have frozen the values $C_i(\mu)$ at $C_i(\mu_0 = 0.5)$ GeV, whenever μ runs to below the scale μ_0, since the renormalization-group (RG) evolution is not reliable for $\mu < \mu_0$. Note that μ_0 is also the scale, which sets the starting point of the RG evolution of the Gegenbauer coefficients in

	$\mathcal{A}^{(u)}_{\pi^+\pi^-}$
F_e	$F_{e4}\,(a_1)$
$\mathcal{M}_e$	$\mathcal{M}_{e4}\,(a_1')$
F_a	0
$\mathcal{M}_a$	$\mathcal{M}_{a4}\,(a_2')$
	$\mathcal{A}^{(t)}_{\pi^+\pi^-}$
F_e^P	$F_{e4}\left(a_4^{(u)}\right) + F_{e6}\left(a_6^{(u)}\right)$
$\mathcal{M}_e^P$	$\mathcal{M}_{e4}\left(a_4^{\prime(u)}\right)$
F_a^P	$F_{a6}\left(a_6^{(d)}\right)$
$\mathcal{M}_a^P$	$\mathcal{M}_{a4}\left(a_3^{\prime(u)} + a_3^{\prime(d)} + a_4^{\prime(d)} + a_5^{\prime(u)} + a_5^{\prime(d)}\right)$
	$\sqrt{2}\mathcal{A}^{(u)}_{\pi^+\pi^0}$
F_e	$F_{e4}\,(a_1 + a_2)$
$\mathcal{M}_e$	$\mathcal{M}_{e4}\,(a_1' + a_2')$
F_a	0
$\mathcal{M}_a$	0
	$\sqrt{2}\mathcal{A}^{(t)}_{\pi^+\pi^0}$
F_e^P	$F_{e4}\left(a_3^{(u)} - a_3^{(d)} + a_4^{(u)} - a_4^{(d)} - a_5^{(u)} + a_5^{(d)}\right) + F_{e6}\left(a_6^{(u)} - a_6^{(d)}\right)$
$\mathcal{M}_e^P$	$\mathcal{M}_{e4}\left(a_3^{\prime(u)} - a_3^{\prime(d)} + a_4^{\prime(u)} - a_4^{\prime(d)} + a_5^{\prime(u)} - a_5^{\prime(d)}\right)$
F_a^P	0
$\mathcal{M}_a^P$	0
	$\sqrt{2}\mathcal{A}^{(u)}_{\pi^0\pi^0}$
F_e	$F_{e4}\,(-a_2)$
$\mathcal{M}_e$	$\mathcal{M}_{e4}\,(-a_2')$
F_a	0
$\mathcal{M}_a$	$\mathcal{M}_{a4}\,(a_2')$
	$\sqrt{2}\mathcal{A}^{(t)}_{\pi^0\pi^0}$
F_e^P	$F_{e4}\left(-a_3^{(u)} + a_3^{(d)} + a_4^{(d)} + a_5^{(u)} - a_5^{(d)}\right) + F_{e6}\left(a_6^{(d)}\right)$
$\mathcal{M}_e^P$	$\mathcal{M}_{e4}\left(-a_3^{\prime(u)} + a_3^{\prime(d)} + a_4^{\prime(d)} - a_5^{\prime(u)} + a_5^{\prime(d)}\right)$
F_a^P	$F_{a6}\left(a_6^{(d)}\right)$
$\mathcal{M}_a^P$	$\mathcal{M}_{a4}\left(a_3^{\prime(u)} + a_3^{\prime(d)} + a_4^{\prime(d)} + a_5^{\prime(u)} + a_5^{\prime(d)}\right)$

TABLE II: $B \to \pi\pi$ decay amplitudes, whose factorization formulas are presented in Appendix.

the meson distribution amplitudes [32]. We have kept the corrections in higher orders of the electroweak coupling α to the Wilson evolution, which were neglected in [33]. Because the effect of the NLO Wilson coefficients is to enhance the penguin amplitude, the branching ratios of the penguin-dominated $B \to \pi K$ modes increase, and the magnitudes of the direct CP asymmetries decrease a bit accordingly. As shown in Eq. (2), The enhanced penguin amplitude P, being destructive to the color-allowed tree amplitude T, renders the $B \to \pi\pi$ branching ratios vary toward the direction favored by the data. The larger subdominant penguin amplitude also increases the magnitudes of the direct CP asymmetries in the $B \to \pi\pi$ decays due to the stronger interference with the dominant tree amplitudes.

As stated before, the LO PQCD predictions for the $B \to \pi K$ branching ratios are consistent with the data, viewing the range spanned by the columns LO and $\mathrm{LO_{NLOWC}}$ in Table III. However, the prediction for the $B^0 \to \pi^0\pi^0$ branching ratio is too small compared to the measured value. Those for the direct CP asymmetries of the $B \to \pi K$, $\pi\pi$ decays, except $A_{CP}(B^\pm \to \pi^0 K^\pm)$, are all in good agreement with the data as shown in Table IV. The LO direct CP asymmetry of the $B^0 \to \pi^0\pi^0$ mode differs in sign from the result obtained in [3], because we have employed the different pion distribution amplitudes (see Sec. IV). It simply implies that the theoretical uncertainty for the modes with tiny branching ratios is huge. Note that the predictions from QCDF [25] for the direct CP asymmetries usually have signs opposite to those from PQCD. It has been realized that the set "S4" with non-universal parameters, such as the different annihilation phases for the $B \to PP$, PV, and VP decays, must be adopted in order for QCDF to accommodate the data [33, 34, 35, 36]. The above two discrepancies associated with the $B^0 \to \pi^0\pi^0$ branching ratio and with the $B^\pm \to \pi^0 K^\pm$ direct CP asymmetry lead to the puzzles mentioned in Introduction. We prepare Table V for the various topological amplitudes, whose definitions are referred to [6]. The values in the columns LO and $\mathrm{LO_{NLOWC}}$ follow the power counting rules in Eqs. (3) and (5) exactly, explaining why the $B \to \pi K$, $\pi\pi$ puzzles appear.

Mode	Data [1]	LO	$\mathrm{LO_{NLOWC}}$	+VC	+QL	+MP	+NLO
$B^\pm \to \pi^\pm K^0$	24.1 ± 1.3	17.0	32.3	31.0	34.2	24.1	$24.5^{+13.6\,(+12.9)}_{-\ 8.1\,(-\ 7.8)}$
$B^\pm \to \pi^0 K^\pm$	12.1 ± 0.8	10.2	18.4	17.4	19.4	14.0	$13.9^{+10.0\,(+\ 7.0)}_{-\ 5.6\,(-\ 4.2)}$
$B^0 \to \pi^\mp K^\pm$	18.9 ± 0.7	14.2	27.7	26.7	29.4	20.5	$20.9^{+15.6\,(+11.0)}_{-\ 8.3\,(-\ 6.5)}$
$B^0 \to \pi^0 K^0$	11.5 ± 1.0	5.7	12.1	11.8	12.8	8.7	$9.1^{+\ 5.6\,(+\ 5.1)}_{-\ 3.3\,(-\ 2.9)}$
$B^0 \to \pi^\mp \pi^\pm$	5.0 ± 0.4	7.0	6.8	6.6	6.9	6.7	$6.5^{+\ 6.7\,(+\ 2.7)}_{-\ 3.8\,(-\ 1.8)}$
$B^\pm \to \pi^\pm \pi^0$	5.5 ± 0.6	3.5	4.1	4.0	4.1	4.1	$4.0^{+\ 3.4\,(+\ 1.7)}_{-\ 1.9\,(-\ 1.2)}$
$B^0 \to \pi^0 \pi^0$	1.45 ± 0.29	0.12	0.27	0.37	0.29	0.21	$0.29^{+0.50\,(+0.13)}_{-0.20\,(-0.08)}$

TABLE III: Branching ratios in the NDR scheme ($\times 10^{-6}$). The label $\mathrm{LO_{NLOWC}}$ means the LO results with the NLO Wilson coefficients, and +VC, +QL, +MP, and +NLO mean the inclusions of the vertex corrections, of the quark loops, of the magnetic penguin, and of all the above NLO corrections, respectively. The errors in the parentheses were defined in the context.

Mode	Data [1]	LO	$\mathrm{LO_{NLOWC}}$	+VC	+QL	+MP	+NLO
$B^\pm \to \pi^\pm K^0$	-0.02 ± 0.04	-0.01	-0.01	-0.01	0.00	-0.01	$0.00 \pm 0.00\,(\pm 0.00)$
$B^\pm \to \pi^0 K^\pm$	0.04 ± 0.04	-0.08	-0.06	-0.01	-0.05	-0.08	$-0.01^{+0.03\,(+0.03)}_{-0.05\,(-0.05)}$
$B^0 \to \pi^\mp K^\pm$	-0.115 ± 0.018	-0.12	-0.08	-0.09	-0.06	-0.10	$-0.09^{+0.06\,(+0.04)}_{-0.08\,(-0.06)}$
$B^0 \to \pi^0 K^0$	0.02 ± 0.13	-0.02	0.00	-0.07	0.00	0.00	$-0.07^{+0.03\,(+0.01)}_{-0.03\,(-0.01)}$
$B^0 \to \pi^\mp \pi^\pm$	0.37 ± 0.10	0.14	0.19	0.21	0.16	0.20	$0.18^{+0.20\,(+0.07)}_{-0.12\,(-0.06)}$
$B^\pm \to \pi^\pm \pi^0$	0.01 ± 0.06	0.00	0.00	0.00	0.00	0.00	$0.00 \pm 0.00\,(\pm 0.00)$
$B^0 \to \pi^0 \pi^0$	$0.28^{+0.40}_{-0.39}$	-0.04	-0.34	0.65	-0.41	-0.43	$0.63^{+0.35\,(+0.09)}_{-0.34\,(-0.15)}$

TABLE IV: Direct CP asymmetries in the NDR scheme.

After obtaining the values of the various topological amplitudes, we compute the mixing-induced CP asymmetries through Eqs. (17) and (20). Since C' is of $O(\lambda^2)$ compared to P', it is expected that the LO PQCD

Topology	LO	LO_{NLOWC}	+VC	+QL	+MP	+NLO
P'	$36.6\,e^{i\,2.9}$	$50.6\,e^{i\,2.9}$	$49.6\,e^{i\,2.9}$	$52.1\,e^{i\,2.9}$	$43.7\,e^{i\,2.8}$	$44.1\,e^{i\,2.9}$
T'	$6.9\,e^{i\,0.0}$	$6.6\,e^{i\,0.0}$	$6.6\,e^{i\,0.1}$	$6.6\,e^{i\,0.0}$	$6.6\,e^{i\,0.0}$	$6.6\,e^{i\,0.1}$
C'	$0.5\,e^{-i\,2.5}$	$0.6\,e^{-i\,0.4}$	$1.9\,e^{-i\,1.3}$	$0.6\,e^{-i\,0.2}$	$0.6\,e^{-i\,0.4}$	$1.7\,e^{-i\,1.3}$
P'_{ew}	$5.8\,e^{i\,3.1}$	$5.8\,e^{-i\,3.1}$	$5.4\,e^{-i\,3.0}$	$5.8\,e^{-i\,3.1}$	$5.8\,e^{-i\,3.1}$	$5.4\,e^{-i\,3.0}$
T	$24.3\,e^{i\,0.0}$	$23.5\,e^{i\,0.0}$	$23.1\,e^{i\,0.0}$	$23.6\,e^{-i\,0.1}$	$23.5\,e^{i\,0.0}$	$23.2\,e^{i\,0.0}$
P	$4.7\,e^{-i\,0.4}$	$6.5\,e^{-i\,0.4}$	$6.3\,e^{-i\,0.3}$	$6.7\,e^{-i\,0.3}$	$5.7\,e^{-i\,0.4}$	$5.6\,e^{-i\,0.4}$
C	$0.8\,e^{i\,2.6}$	$2.2\,e^{i\,0.2}$	$4.8\,e^{-i\,1.1}$	$2.3\,e^{i\,0.4}$	$2.2\,e^{i\,0.2}$	$4.3\,e^{-i\,1.1}$
P_{ew}	$0.7\,e^{i\,0.0}$	$0.7\,e^{i\,0.0}$	$0.7\,e^{-i\,0.1}$	$0.7\,e^{i\,0.0}$	$0.7\,e^{i\,0.0}$	$0.7\,e^{-i\,0.1}$

TABLE V: Topological amplitudes in units of 10^{-5} GeV for the $B \to \pi K$, $\pi\pi$ decays in the NDR scheme.

	Data	LO	LO_{NLOWC}	+VC	+QL	+MP	+NLO
$S_{\pi^0 K_S}$	0.31 ± 0.26	0.70	0.73	0.74	0.73	0.73	$0.74^{+0.02\,(+0.01)}_{-0.03\,(-0.01)}$
$S_{\pi\pi}$	-0.50 ± 0.12	-0.34	-0.49	-0.47	-0.51	-0.41	$-0.42^{+1.00\,(+0.05)}_{-0.56\,(-0.05)}$

TABLE VI: Mixing-induced CP asymmetries in the NDR scheme.

results of $S_{\pi^0 K_S}$ are close to that extracted from the $b \to c\bar{c}s$ decays, $S_{c\bar{c}s} = \sin(2\phi_1) \approx 0.685$, as shown in Table VI. On the contrary, P is of $O(\lambda)$ of T in the $B^0 \to \pi^\mp\pi^\pm$ decays, such that a larger deviation of $S_{\pi\pi}$ from $S_{c\bar{c}s}$ is found. The LO PQCD results of $S_{\pi\pi}$ are consistent with the data, but those of $S_{\pi^0 K_S}$ are not. Moreover, PQCD predicts $\Delta S_{\pi^0 K_S} \equiv S_{\pi^0 K_S} - S_{c\bar{c}s} > 0$, opposite to the observed values. This result is in agreement with those obtained in the literature [15, 37, 38]. Hence, the measurement of the mixing-induced CP asymmetries in the penguin-dominated modes provides an opportunity of discovering new physics. Currently, the data of $S_{\pi^0 K_S}$ still suffer significant errors. On the other hand, the NLO corrections and the theoretical uncertainty, which concern the allowed range of the PQCD predictions, need to be analyzed. A more clear picture will be attained, after we complete these analyses.

III. NEXT-TO-LEADING-ORDER CORRECTIONS

We explain the consistent power countings in α_s and in large logarithms, before computing the NLO corrections. A PQCD formula of leading-power in $1/m_b$ is written symbolically as

$$\exp[\gamma^{(0)}(\alpha_s)L_{WC}] \otimes \exp[\Gamma^{(0)}(\alpha_s)L_S^2 + \Gamma^{(1)}(\alpha_s^2)L_S^2] \otimes \exp[\gamma_q^{(0)}(\alpha_s)L_{RG}] \otimes H^{(0)}(\alpha_s) \otimes \phi(\mu_0)\ , \tag{22}$$

where the first, second, and third exponentials represent the Wilson coefficient, the Sudakov factor, and the RG factor [39], with the notations $L_{WC} \equiv \ln(m_W/t)$, $L_S \equiv \ln(xPb)$, and $L_{RG} \equiv \ln(tb)$, xP being a fractional parton momentum, $t \sim \sqrt{\bar{\Lambda} m_b}$ a characteristic hard scale, and b the conjugate variable to the parton transverse momentum k_T, and γ, Γ, and γ_q the corresponding anomalous dimensions. The RG factor governs the evolution from t down to $1/b$. The evolution from $1/b$ down to the cutoff μ_0, which characterizes the meson distribution amplitude ϕ, has been neglected. This formula is complete at LO, since the hard kernel H is evaluated to $O(\alpha_s)$, and at next-to-leading logarithm (NLL), since the Wilson coefficient, the Sudakov factor, and the RG factor have been resummed up to the next-to-leading logarithms $\alpha_s L_{WC}$, $\alpha_s L_S$, and $\alpha_s L_{RG}$, respectively ($\alpha_s L_S^2$ is the leading logarithm). In all our previous works we used the one-loop running coupling constant α_s, which is, strictly speaking, a NLO effect. This effect takes into account the potential large NLO corrections to the B meson transition form factors through the BLM procedure (see Introduction).

Next, we add subleading corrections to Eq. (22), which include

1. $H^{(0)}(\alpha_s) \to H^{(0)}(\alpha_s) + H^{(1)}(\alpha_s^2)$. This is what we are going to do in this section, where the NLO hard kernel $H^{(1)}$ contains the vertex corrections, the quark loops, and the magnetic penguin.

2. $\exp[\gamma^{(0)}(\alpha_s)L_{WC}] \to \exp[\gamma^{(0)}(\alpha_s)L_{WC} + \gamma^{(1)}(\alpha_s^2)L_{WC}]$. The LO Wilson coefficient is replaced by the NLO one, for which the corresponding anomalous dimension is calculated to two loops: $\gamma^{(0)}(\alpha_s) \to \gamma^{(0)}(\alpha_s)+\gamma^{(1)}(\alpha_s^2)$. According to our counting rules, the NLO anomalous dimension leads to the summation of the next-to-next-to-leading logarithm (NNLL) $\alpha_s^2 L_{WC}$.

3. $\exp[\Gamma^{(0)}(\alpha_s)L_S^2 + \Gamma^{(1)}(\alpha_s^2)L_S^2] \to \exp[\Gamma^{(0)}(\alpha_s)L_S^2 + \Gamma^{(1)}(\alpha_s^2)L_S^2 + \Gamma^{(2)}(\alpha_s^3)L_S^2]$. This means the accuracy of the summation up to NNLL ($\alpha_s^3 L_S^2$). Unfortunately, it requires a three-loop evaluation of the corresponding anomalous dimension for the Sudakov factor, which is not yet available in the literature.

4. $\exp[\gamma_q^{(0)}(\alpha_s)L_{RG}] \to \exp[\gamma_q^{(0)}(\alpha_s)L_{RG} + \gamma_q^{(1)}(\alpha_s^2)L_{RG}]$. Since L_{RG} and L_S are of the same order of magnitude, and the NNLL Sudakov resummation is not available, this NNLL piece of subleading corrections ($\alpha_s^2 L_{RG}$) can not be included consistently.

The power countings in α_s and in various large logarithms are independent in principle. Based on the above classification, we shall extend Eq. (22) by considering the subleading corrections from the first and second pieces. With the one-loop running α_s, the NLO corrections to the hard kernel are complete (assuming that the corrections to the form factors have been minimized by our choice of the hard scale). It is not necessary to adopt the two-loop α_s as in [33], whose effect is next-to-next-to-leading-order (NNLO). Because of $L_{WC} \gg L_S, L_{RG}$, the NNLL term $\alpha_s^2 L_{WC}$ is much more essential than those from the third and fourth pieces. The LO PQCD results for the $B \to \pi K$, $\pi\pi$ decays from using the NLO Wilson coefficients have been listed in Tables III-VI. When investigating the NLO corrections from the vertex corrections, the quark loops, and the magnetic penguin to the hard kernel below, we shall always use the NLO Wilson coefficients. After obtaining the decay amplitudes $\mathcal{A}(B \to f)$ up to NLO, we employ Eq. (14) to evaluate the corresponding decay rates.

A. Vertex Corrections

It has been known that the vertex corrections, reducing the dependence of the Wilson coefficients on the renormalization scale μ, play an important role in a NLO analysis. Since the nonfactorizable contributions are negligible [40], we concentrate only on the vertex corrections to the factorizable amplitudes. For charmless B meson decays, these corrections do not involve the end-point singularities from vanishing momentum fractions in collinear factorization theorem (QCDF [25]). Therefore, there is no need to employ k_T factorization theorem (PQCD [2, 3, 39, 41, 42]) here. This claim can be justified by recalculating one of the nonfactorizable amplitudes, $\mathcal{M}_{e4}$, for the $B \to \pi K$ decays in collinear factorization theorem, which is also free of the end-point singularity. It is found that the results for $\mathcal{M}_{e4}$ from the two calculations (with and without the parton transverse momentum k_T in the kaon) differ only by 10%. For more detail, refer to Appendix. After justifying the neglect of the parton transverse degrees of freedom, we simply quote the QCDF expressions for the vertex corrections. An important remark is that the light quark from the b quark transition is assumed to carry the full momentum of the associated meson in QCDF [25]. Strictly speaking, this light quark carries the fractional momentum, whose dependence should appear in the PQCD formalism for the vertex corrections. Because it is indeed an energetic quark, the assumption is reasonable.

The vertex corrections modify the Wilson coefficients in Eq. (12) into [25]

$$\begin{aligned}
a_1(\mu) &\to a_1(\mu) + \frac{\alpha_s(\mu)}{4\pi} C_F \frac{C_1(\mu)}{N_c} V_1(M) \,, \\
a_2(\mu) &\to a_2(\mu) + \frac{\alpha_s(\mu)}{4\pi} C_F \frac{C_2(\mu)}{N_c} V_2(M) \,, \\
a_i(\mu) &\to a_i(\mu) + \frac{\alpha_s(\mu)}{4\pi} C_F \frac{C_{i\pm1}(\mu)}{N_c} V_i(M) \,, \quad i = 3 - 10,
\end{aligned} \tag{23}$$

with M being the meson emitted from the weak vertex. For the $B \to \pi K$ decays, M denotes the kaon for the

vertex functions $V_{1,4,6,8,10}$ and the pion for $V_{2,3,5,7,9}$. In the NDR scheme $V_i(M)$ are given by [25]

$$V_i(M) = \begin{cases} 12\ln\dfrac{m_b}{\mu} - 18 + \dfrac{2\sqrt{2N_c}}{f_M}\displaystyle\int_0^1 dx\,\phi_M^A(x)\,g(x)\;, & \text{for } i = 1-4, 9, 10\;, \\ -12\ln\dfrac{m_b}{\mu} + 6 - \dfrac{2\sqrt{2N_c}}{f_M}\displaystyle\int_0^1 dx\,\phi_M^A(x)\,g(1-x)\;, & \text{for } i = 5, 7\;, \\ -6 + \dfrac{2\sqrt{2N_c}}{f_M}\displaystyle\int_0^1 dx\,\phi_M^P(x)\,h(x)\;, & \text{for } i = 6, 8\;, \end{cases} \tag{24}$$

where f_M is the decay constant of the meson M, and $\phi_M^A(x)$ $[\phi_M^P(x)]$ the twist-2 (twist-3) meson distribution amplitude given in Sec. IV, x being the parton momentum fraction. The hard kernels are

$$\begin{aligned} g(x) &= 3\left(\frac{1-2x}{1-x}\ln x - i\,\pi\right) \\ &\quad + \left[2\,\mathrm{Li}_2(x) - \ln^2 x + \frac{2\ln x}{1-x} - (3+2i\,\pi)\ln x - (x \leftrightarrow 1-x)\right]\;, \end{aligned} \tag{25}$$

$$h(x) = 2\,\mathrm{Li}_2(x) - \ln^2 x - (1+2i\,\pi)\ln x - (x \leftrightarrow 1-x)\;. \tag{26}$$

The expressions of $V_i(M)$ in the HV scheme can be found in [43]. The factorization formulas for the various $B \to \pi K$, $\pi\pi$ decay amplitudes are still the same as in Tables I and II.

The dependence of the Wilson coefficients $a_i(\mu)$ on the renormalization scale μ modified by the vertex corrections is exhibited in Fig. 1 for both the real and imaginary parts. It is found that the μ dependence of most of a_i is moderated by the vertex corrections (with the generation of the imaginary parts). The μ dependence of $a_{6,8}$ is, however, not altered. It has been known that their dependence will be moderated after combined with the μ dependence of the chiral scale $m_{0K}(\mu)$ associated with the kaon [25]. The most dramatic changes arise from $a_{2,3,10}$. Due to the smallness of a_3 (a_{10}) compared to the Wilson coefficient $a_{4,6}$ (a_9) for the QCD (electroweak) penguins, the only significant effect appears in the color-suppressed tree amplitude C', which is governed by a_2. For other a_i, the vertex corrections amount only up to 70% at the scale $\mu \sim \sqrt{\bar{\Lambda} m_b} \sim 1.5$ GeV. The above observation is manifest in Table V: most of the topological amplitudes for the $B \to \pi K$, $\pi\pi$ decays change a little, while C' and C are enhanced by factors of 3 and 2 (viewing the values in the columns $\mathrm{LO_{NLOWC}}$ and +VC), respectively.

It is then understood that the $B \to \pi K$ branching ratios, dominated by the penguin contributions from $a_{4,6}$, vary only slightly under the vertex corrections, as indicated in Table III. However, the direct CP asymmetries of the $B^\pm \to \pi^0 K^\pm$ and $B^0 \to \pi^0 K^0$ modes, related to C', are modified significantly, as shown in Tables IV: $A_{CP}(B^\pm \to \pi^0 K^\pm)$ has increased from -0.06 to -0.01, and $A_{CP}(B^0 \to \pi^0 K^0) \equiv A_{\pi^0 K_S}$ has decreased from 0.00 to -0.07. $A_{CP}(B^0 \to \pi^\mp K^\pm)$, determined solely by the color-allowed tree amplitude T', does not change much. The effect from the vertex corrections on the LO PQCD predictions for the $B \to \pi\pi$ decays can also be understood by means of the enhanced color-suppressed tree amplitude C: the $B^0 \to \pi^0\pi^0$ branching ratio increases by 30%, and the direct CP asymmetry changes from -0.34 to $+0.65$. The sign flip of the direct CP asymmetry is attributed to a huge change of the strong phase of C caused by the vertex corrections. The predicted $B^0 \to \pi^\pm\pi^\mp$ and $B^\pm \to \pi^\pm\pi^0$ branching ratios, to which C remains subdominant, decrease only a bit. The NLO effect, though increasing $|C|$ by a factor of 2, is not enough to resolve the $B \to \pi\pi$ puzzle. Perhaps, the penguin amplitude is also larger than expected [30, 44]. Nevertheless, the vertex corrections do improve the consistency between the theoretical predictions and the experimental data of the $B \to \pi\pi$ decays.

Though the vertex corrections have been included in QCDF [25], they do not help resolve the $B \to \pi K$ puzzle. We neglect the electroweak penguin P'_{ew} for convenience in the following explanation. Table V shows that the penguin amplitude P' is in the second quadrant, and the color-allowed tree amplitude T' is roughly aligned with the positive real axis. The color-suppressed tree amplitude C' is enhanced by the vertex corrections, and becomes almost imaginary. It then orients the sum $T' + C'$ into the fourth quadrant, such that $T' + C'$ and P' more or less line up (and point to the opposite directions). This is the reason the magnitude of $A_{CP}(B^\pm \to \pi^0 K^\pm)$, proportional to the sine of the angle between $T' + C'$ and P', becomes smaller in PQCD. The situation in QCDF is different, where P' is preferred to be in the third quadrant [40]. That is, the predicted $A_{CP}(B^0 \to \pi^\mp K^\pm)$ has a wrong sign. Then the modified C', still orienting $T' + C'$ into the fourth quadrant, can not reduce the magnitude of $A_{CP}(B^\pm \to \pi^0 K^\pm)$. The three types of NLO corrections considered here have been extended up

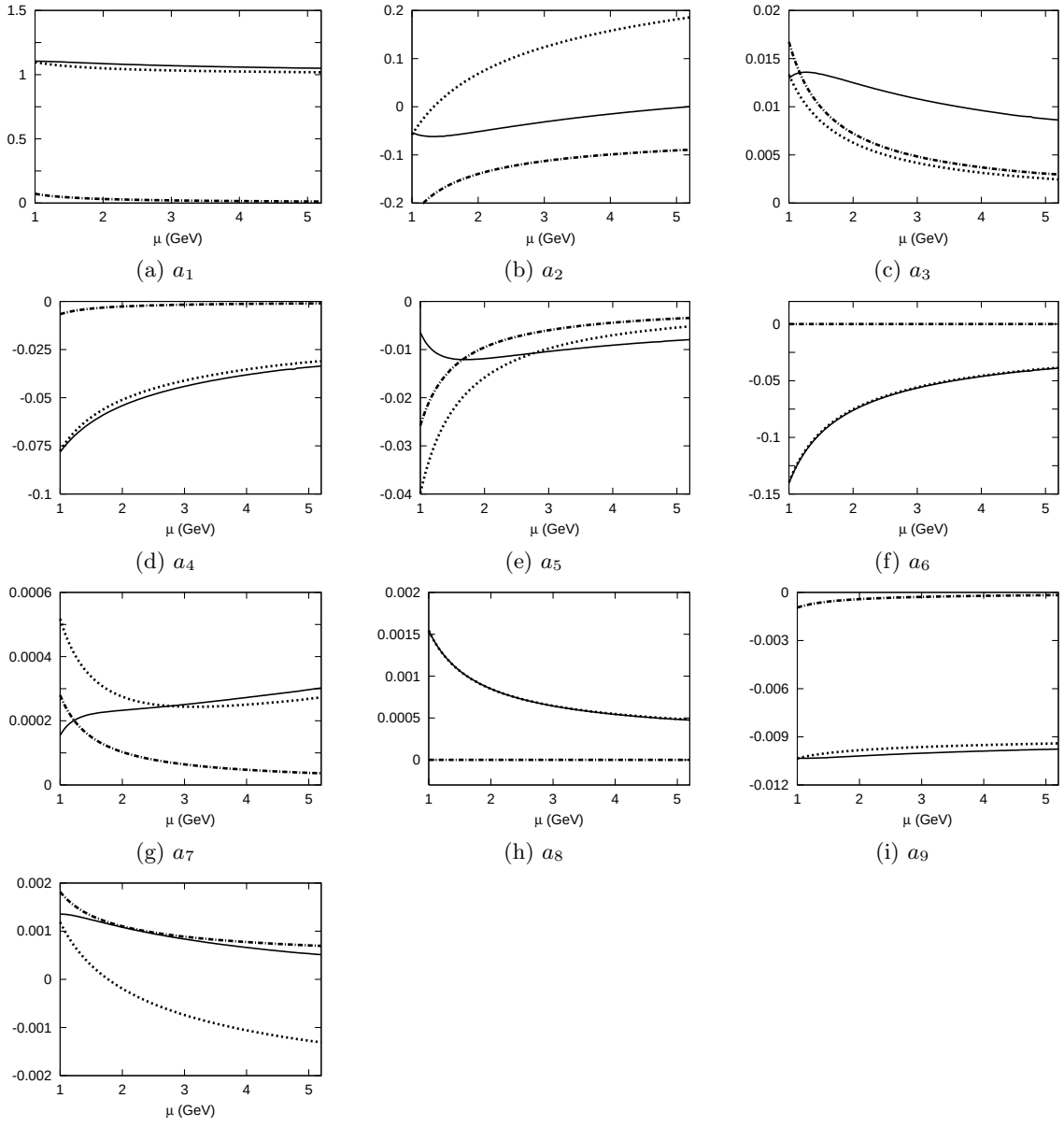

(a) a_1 (b) a_2 (c) a_3

(d) a_4 (e) a_5 (f) a_6

(g) a_7 (h) a_8 (i) a_9

(g) a_{10}

FIG. 1: Real parts of a_i for the $B \to \pi K$ decays without the vertex corrections (dotted lines) and with the vertex corrections (solid lines), and imaginary parts with the vertex corrections (dot-dashed lines) in the NDR scheme.

to $O(\alpha_s^2\beta_0)$ in QCDF recently [45], which, however, make the QCDF predictions for $A_{CP}(B^\pm \to \pi^0 K^\pm)$ more deviate from the data. Another $O(\alpha_s^2)$ piece from the $b \to sg^*g^*$ transition was included into QCDF [46], which enhances the $B \to \pi K$ branching ratios, but leaves their direct CP asymmetries intact. The $B \to \pi K$ puzzle can not be resolved in SCET either [47]: the leading SCET formalism requires the ratio C'/T' to be real, so that C', being parallel to T', can not orient the sum $T' + C'$ into the fourth quadrant, and that the magnitude of $A_{CP}(B^\pm \to \pi^0 K^\pm)$ remains large.

We have found that the color-suppressed tree amplitude C' could be enhanced few times by the vertex corrections in the standard model. It is then worthwhile to investigate whether the mixing-induced CP asymmetry $S_{\pi^0 K_S}$ in the $B \to \pi^0 K_S$ decays deviates from $S_{c\bar{c}s}$ substantially under a large C' according to Eq. (17). A

similar investigation of the large C effect applies to $S_{\pi\pi}$ in the $B^0 \to \pi^\mp\pi^\pm$ decays according to Eq. (20). The results are collected in Table VI, which indicates that the deviation is still small and positive. It is known that the leading deviation caused by C' is proportional to $\cos(\delta_{C'} - \delta_{P'})$, if neglecting P'_{ew}. Because the vertex corrections also rotate the orientation of C', it becomes more orthogonal to P' as shown in Table V, and $\Delta S_{\pi^0 K_S}$ is not increased much. The mixing-induced CP asymmetry $S_{\pi\pi}$, depending only on T and P, is insensitive to the vertex corrections, which mainly affect C.

B. Quark Loops

For the $B \to \pi K$ and $B \to \pi\pi$ decays, the dominant penguin amplitude $P' \sim |V_{tb}V_{ts}^*|C_4$ and tree amplitude $T \sim |V_{ub}V_{ud}^*|C_2$ are both of $O(\lambda^4)$ [13]. Hence, the charm-quark loop amplitude, proportional to $\alpha_s|V_{cb}V_{cs}^*|C_2 \sim \alpha_s\lambda^2$ in the former and to $\alpha_s|V_{cb}V_{cd}^*|C_2 \sim \alpha_s\lambda^3$ in the latter, could be an important source of NLO corrections. Its effect is expected to be larger in the $B \to \pi K$ decays. On the other hand, the up-quark loop amplitude, proportional to $\alpha_s|V_{ub}V_{us}^*|C_2 \sim \alpha_s\lambda^5$ [13] for $B \to \pi K$, seems to be negligible. For $B \to \pi\pi$, the up-quark loop amplitude, proportional to $\alpha_s|V_{ub}V_{ud}^*|C_2 \sim \alpha_s\lambda^4$ [13], might be comparable to the charm-quark one. Therefore, we shall include both quark loops in the following analysis. For completeness, we shall also include the quark-loop amplitudes from the QCD penguin operators, whose contributions are proportional to $\alpha_s|V_{tb}V_{ts}^*|C_i \sim \alpha_s\lambda^4$, $i = 3, 4, 6$. They have the order of magnitude the same as or larger than the up-quark one, and can influence the direct CP asymmetries of the $B \to \pi K$ modes. The quark loops from the electroweak penguins will be neglected due to their smallness. Note that the CKM factors of these corrections differ among the loop amplitudes and between the $b \to s(d)$ and $\bar{b} \to \bar{s}(\bar{d})$ transitions.

For the $b \to s$ transition, the contributions from the various quark loops are given by

$$H_{\rm eff} \;=\; -\sum_{q=u,c,t}\sum_{q'}\frac{G_F}{\sqrt{2}}V_{qb}V_{qs}^*\frac{\alpha_s(\mu)}{2\pi}C^{(q)}(\mu,l^2)\,(\bar{s}\gamma_\rho(1-\gamma_5)T^a b)\,(\bar{q}'\gamma^\rho T^a q')\;, \tag{27}$$

l^2 being the invariant mass of the gluon, which attaches the quark loops in Fig. 2. For the $b \to d$ transition, the quark-loop corrections are obtained by substituting d for s in Eq. (27). The functions $C^{(q)}(\mu, l^2)$ are written as

$$C^{(q)}(\mu,l^2) \;=\; \left[G^{(q)}(\mu,l^2) - \frac{2}{3}\right] C_2(\mu)\;, \tag{28}$$

for $q = u$, c, and

$$C^{(t)}(\mu,l^2) \;=\; \left[G^{(s)}(\mu,l^2) - \frac{2}{3}\right] C_3(\mu) \;+\; \sum_{q''=u,d,s,c} G^{(q'')}(\mu,l^2)\,[C_4(\mu) + C_6(\mu)]\;. \tag{29}$$

The constant term $-2/3$ in the above expressions arises from the Fierz transformation of the four-fermion operators in D dimensions with the anti-commuting Dirac matrix γ_5 in the NDR scheme. The contribution proportional to the Wilson coefficient C_5, being purely ultraviolet, should be combined with that from the magnetic penguin to form the effective Wilson coefficient $C_{8g} + C_5$ [31]. Since our characteristic hard scale is of order $\sqrt{\bar{\Lambda} m_b} \sim 1.5$ GeV, the b quark is not an active one, and does not contribute to Eq. (29). Except this difference, our expressions are basically the same as in [25].

The function $G^{(c)}(\mu, l^2)$ for the loop of the massive charm quark is given by

$$G^{(c)}(\mu,l^2) \;=\; -4\int_0^1 dx\, x(1-x)\ln\frac{m_c^2 - x(1-x)l^2}{\mu^2}\;, \tag{30}$$

m_c being the charm quark mass, whose real and imaginary parts are

$$\mathrm{Re}\, G^{(c)}(\mu,l^2) \;=\; \frac{2}{3}\left(\frac{5}{3} + \frac{4m_c^2}{l^2} - \ln\frac{m_c^2}{\mu^2}\right)$$

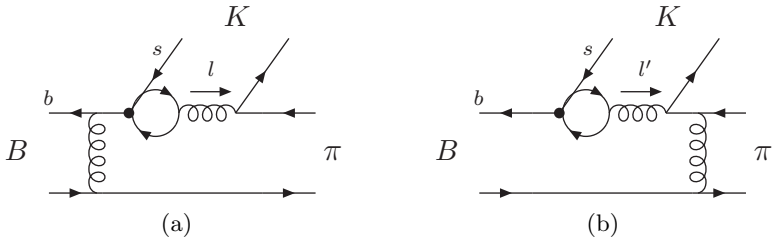

FIG. 2: Quark-loop amplitudes.

$$+\frac{2}{3}\left(1+\frac{2m_c^2}{l^2}\right)\begin{cases}\sqrt{1-\frac{4m_c^2}{l^2}}\ln\frac{\sqrt{1-\frac{4m_c^2}{l^2}}-1}{\sqrt{1-\frac{4m_c^2}{l^2}}+1}\,, & -\infty<l^2<0\\ -2\sqrt{\frac{4m_c^2}{l^2}-1}\cot^{-1}\left(\sqrt{\frac{4m_c^2}{l^2}-1}\right)\,, & 0\le l^2<4m_c^2\\ -2\left(1-\frac{4m_c^2}{l^2}\right)\,, & l^2=4m_c^2\\ \sqrt{1-\frac{4m_c^2}{l^2}}\ln\frac{1-\sqrt{1-\frac{4m_c^2}{l^2}}}{1+\sqrt{1-\frac{4m_c^2}{l^2}}}\,, & 4m_c^2<l^2<\infty\end{cases} \tag{31}$$

and

$$\mathrm{Im}\,G^{(c)}(\mu,l^2)\;=\;\frac{2\pi}{3}\left(1+\frac{2m_c^2}{l^2}\right)\sqrt{1-\frac{4m_c^2}{l^2}}\,\theta\left(1-\frac{4m_c^2}{l^2}\right)\,, \tag{32}$$

respectively. For the loops of the light quarks u, d, and s, we have the expressions similar to Eq. (30) but with m_c being replaced by m_u, m_d, and m_s, respectively. Because their contributions are insensitive to the light quark masses, we simply adopt the same mass m for the three quark loops. Varying m from $m_u = 4.5$ MeV to $m_s \approx 100$ MeV, the branching ratios change by less than 1%.

To picture the quark-loop effect, we display in Fig. 3 the dependence of $[V_{qb}V^*_{qs(d)}/(V_{tb}V^*_{ts(d)})]C^{(q)}$, $q = u, c, t$, on the renormalization scale μ for a given $l^2 = m_B^2/4$ in the NDR scheme. The real part of the up-quark loop is indeed negligible compared to that of the charm-quark loop in the $b \to s$ transition as indicated in Fig. 3(a). However, in the other transitions described by Figs. 3(b)-3(d), the up- and charm-loop corrections are comparable as argued above. The quark loops from the QCD penguin operators are in fact essential. Figures 3(a) and 3(c) [and also Figs. 3(b) and 3(d)] imply that the weak phases cause different μ dependences between the $b \to s$ and $b \to d$ transitions in the cases of the up and charm loops, but not in the case of the QCD-penguin loops.

The quark-loop amplitudes depend on the gluon invariant mass l^2, which is assumed to be an arbitrary constant $\langle l^2\rangle$ in FA. Since the topology displayed in Fig. 2 is the same as the penguin one, its contribution can be absorbed into the Wilson coefficients $a_{4,6}$,

$$a_{4,6}(\mu)\;\to\;a_{4,6}(\mu)+\frac{\alpha_s(\mu)}{9\pi}\sum_{q=u,c,t}\frac{V_{qb}V^*_{qs(d)}}{V_{tb}V^*_{ts(d)}}C^{(q)}(\mu,\langle l^2\rangle)\,, \tag{33}$$

with the other a_i unmodified. The resultant values of $a_{4,6}$ at $\mu = 1.5$ and 4.4 GeV are listed in Table VII. As $\mu = 1.5$ GeV, the quark-loop corrections do not change $a_{4,6}$ much for $b \to s$ and $\bar{b} \to \bar{s}$, while they are destructive (constructive) to $a_{4,6}$ for $b \to d$ ($\bar{b} \to \bar{d}$). As $\mu = 4.4$ GeV, these corrections are always constructive for the different b quark transitions. Besides, the quark-loop corrections are mode-dependent. For example, they cancel between the $u\bar{u}$ and $d\bar{d}$ components of $\pi^0 = (u\bar{u} - d\bar{d})/\sqrt{2}$ in the $B^\pm \to \pi^\pm\pi^0$ decays, but do not in others.

The assumption of a constant gluon invariant mass in FA introduces a large theoretical uncertainty as making predictions. In the more sophisticated PQCD approach, the gluon mass is related to the parton momenta

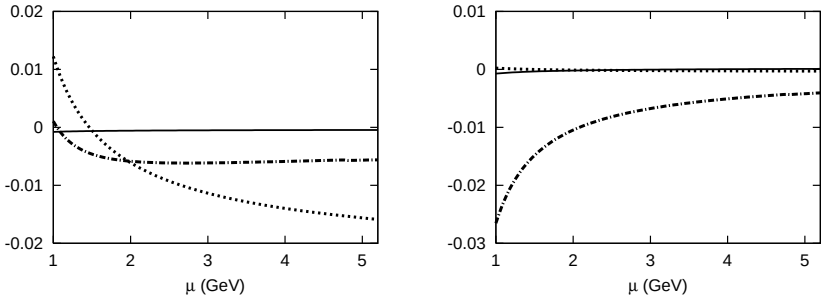

(a) $\mathrm{Re}\left[\frac{\alpha_s(\mu)}{9\pi}\,\frac{V_{qb}V_{qs}^*}{V_{tb}V_{ts}^*}\,C^{(q)}(\mu,l^2)\right]$ (b) $\mathrm{Im}\left[\frac{\alpha_s(\mu)}{9\pi}\,\frac{V_{qb}V_{qs}^*}{V_{tb}V_{ts}^*}\,C^{(q)}(\mu,l^2)\right]$

(c) $\mathrm{Re}\left[\frac{\alpha_s(\mu)}{9\pi}\,\frac{V_{qb}V_{qd}^*}{V_{tb}V_{td}^*}\,C^{(q)}(\mu,l^2)\right]$ (d) $\mathrm{Im}\left[\frac{\alpha_s(\mu)}{9\pi}\,\frac{V_{qb}V_{qd}^*}{V_{tb}V_{td}^*}\,C^{(q)}(\mu,l^2)\right]$

FIG. 3: Quark-loop contributions to the $b \to s$[(a) and (b)] and $b \to d$[(c) and (d)] transitions for $l^2 = m_B^2/4$ with the solid, dotted, and dot-dashed lines corresponding to the up-quark, charm-quark, and QCD-penguin loops, respectively.

	$\mathrm{LO_{NLOWC}}$	+QL ($b \to s$)	+QL ($b \to d$)	+MP
$a_4(1.5\ \mathrm{GeV})$	-0.0601	$-0.0659 - i\,0.0152$	$-0.0500 - i\,0.0131$	-0.0492
$a_6(1.5\ \mathrm{GeV})$	-0.0952	$-0.1010 - i\,0.0152$	$-0.0850 - i\,0.0131$	-0.0843
$a_4(4.4\ \mathrm{GeV})$	-0.0336	$-0.0545 - i\,0.0048$	$-0.0454 - i\,0.0036$	-0.0279
$a_6(4.4\ \mathrm{GeV})$	-0.0428	$-0.0637 - i\,0.0048$	$-0.0546 - i\,0.0036$	-0.0371
	$\mathrm{LO_{NLOWC}}$	+QL ($\bar{b} \to \bar{s}$)	+QL ($\bar{b} \to \bar{d}$)	+MP
$a_4(1.5\ \mathrm{GeV})$	-0.0601	$-0.0646 - i\,0.0150$	$-0.0804 - i\,0.0180$	-0.0492
$a_6(1.5\ \mathrm{GeV})$	-0.0952	$-0.0997 - i\,0.0150$	$-0.1155 - i\,0.0180$	-0.0843
$a_4(4.4\ \mathrm{GeV})$	-0.0336	$-0.0537 - i\,0.0047$	$-0.0628 - i\,0.0065$	-0.0279
$a_6(4.4\ \mathrm{GeV})$	-0.0428	$-0.0630 - i\,0.0047$	$-0.0720 - i\,0.0065$	-0.0371

TABLE VII: $a_{4,6}$ including the quark loops and the magnetic penguin for $l^2 = m_B^2/4$ in the NDR scheme.

unambiguously (see Appendix). Due to the absence of the end-point singularities associated with $l^2, l'^2 \to 0$ in Figs. 2(a) and 2(b), respectively, we have dropped the parton transverse momenta k_T in l^2, l'^2 for simplicity.

The amplitudes in Eq. (9) become

$$\begin{aligned}
&\mathcal{A}^{(u,c)}_{\pi^+K^0} \to \mathcal{A}^{(u,c)}_{\pi^+K^0} + \mathcal{M}^{(u,c)}_{\pi K} , \quad \mathcal{A}^{(t)}_{\pi^+K^0} \to \mathcal{A}^{(t)}_{\pi^+K^0} - \mathcal{M}^{(t)}_{\pi K} , \\
&\mathcal{A}^{(u,c)}_{\pi^0K^+} \to \mathcal{A}^{(u,c)}_{\pi^0K^+} + \frac{1}{\sqrt{2}}\mathcal{M}^{(u,c)}_{\pi K} , \ \mathcal{A}^{(t)}_{\pi^0K^+} \to \mathcal{A}^{(t)}_{\pi^0K^+} - \frac{1}{\sqrt{2}}\mathcal{M}^{(t)}_{\pi K} , \\
&\mathcal{A}^{(u,c)}_{\pi^-K^+} \to \mathcal{A}^{(u,c)}_{\pi^-K^+} + \mathcal{M}^{(u,c)}_{\pi K} , \quad \mathcal{A}^{(t)}_{\pi^-K^+} \to \mathcal{A}^{(t)}_{\pi^-K^+} - \mathcal{M}^{(t)}_{\pi K} , \\
&\mathcal{A}^{(u,c)}_{\pi^0K^0} \to \mathcal{A}^{(u,c)}_{\pi^0K^0} - \frac{1}{\sqrt{2}}\mathcal{M}^{(u,c)}_{\pi K} , \ \mathcal{A}^{(t)}_{\pi^0K^0} \to \mathcal{A}^{(t)}_{\pi^0K^0} + \frac{1}{\sqrt{2}}\mathcal{M}^{(t)}_{\pi K} , \\
&\mathcal{A}^{(u,c)}_{\pi^+\pi^-} \to \mathcal{A}^{(u,c)}_{\pi^+\pi^-} + \mathcal{M}^{(u,c)}_{\pi\pi} , \quad \mathcal{A}^{(t)}_{\pi^+\pi^-} \to \mathcal{A}^{(t)}_{\pi^+\pi^-} - \mathcal{M}^{(t)}_{\pi\pi} , \\
&\mathcal{A}^{(u,c,t)}_{\pi^+\pi^0} \to \mathcal{A}^{(u,c,t)}_{\pi^+\pi^0} , \\
&\mathcal{A}^{(u,c)}_{\pi^0\pi^0} \to \mathcal{A}^{(u,c)}_{\pi^0\pi^0} + \frac{1}{\sqrt{2}}\mathcal{M}^{(u,c)}_{\pi\pi} , \quad \mathcal{A}^{(t)}_{\pi^0\pi^0} \to \mathcal{A}^{(t)}_{\pi^0\pi^0} - \frac{1}{\sqrt{2}}\mathcal{M}^{(t)}_{\pi\pi} ,
\end{aligned} \tag{34}$$

where $\mathcal{M}^{(u)}_f$, $\mathcal{M}^{(c)}_f$ and $\mathcal{M}^{(t)}_f$ denote the up-, charm-, and QCD-penguin-loop corrections, respectively, and the minus sign for the final state π^0K^0 comes from the $d\bar{d}$ component in π^0. The factorization formulas for $\mathcal{M}^{(u,c,t)}_{\pi K}$ and $\mathcal{M}^{(u,c,t)}_{\pi\pi}$ are presented in Appendix.

As indicated in Eq. (33), the quark-loop corrections affect the penguin contributions, but have a minor impact on other topological amplitudes. This observation is clear in Table V: $|P'|$ ($|P|$) has increased from 50.6 to 52.1 (6.5 to 6.7) in the NDR scheme. Since the $B \to \pi K$ decays are penguin-dominated, their branching ratios receive an enhancement (see Table III). The increase of the branching ratios then reduces the magnitude of the direct CP asymmetries in the $B \to \pi K$ modes slightly as shown in Table IV. It is also easy to understand the insensitivity of the mixing-induced CP asymmetry $S_{\pi^0K_S}$ to the quark-loop corrections (see Table VI), viewing the small change in the dominant amplitude P' in Eq. (17). On the contrary, the penguin contribution is subdominant in the $B \to \pi\pi$ decays, so the branching ratios do not vary much. However, the direct CP asymmetries $A_{CP}(B^0 \to \pi^\mp\pi^\pm)$ and $A_{CP}(B^0 \to \pi^0\pi^0)$, and the mixing-induced CP asymmetry $S_{\pi\pi}$, directly related to the penguin amplitude, change sizably.

C. Magnetic Penguins

We then discuss the NLO corrections from the magnetic penguin, whose weak effective Hamiltonian contains the $b \to sg$ transition,

$$H_{\rm eff} = -\frac{G_F}{\sqrt{2}} V_{tb}V^*_{ts} C_{8g} O_{8g} , \tag{35}$$

with the magnetic penguin operator,

$$O_{8g} = \frac{g}{8\pi^2} m_b \bar{s}_i \sigma_{\mu\nu}(1+\gamma_5) T^a_{ij} G^{a\mu\nu} b_j , \tag{36}$$

i, j being the color indices. The Hamiltonian for the $b \to d$ transition is obtained by changing s into d in Eq. (35). The topology of the magnetic penguin operator is similar to that of the quark loops. If regarding the invariant mass l^2 of the gluon emitted from the operator O_{8g} as a constant $\langle l^2\rangle$, the magnetic-penguin contribution to the $B \to \pi K$, $\pi\pi$ decays can also be included into the Wilson coefficients, similar to Eq. (33),

$$a_{4,6}(\mu) \to a_{4,6}(\mu) - \frac{\alpha_s(\mu)}{9\pi} \frac{2m_B}{\sqrt{\langle l^2\rangle}} C^{\rm eff}_{8g}(\mu) , \tag{37}$$

with the effective Wilson coefficient $C^{\rm eff}_{8g} = C_{8g} + C_5$ [31]. The resultant Wilson coefficients $a_{4,6}(\mu)$ for $\mu = 1.5$ and 4.4 GeV have been presented in Table VII. The cancellation between the real parts of the quark-loop corrections and of the magnetic penguin is obvious, except in the case of the $b \to d$ transition for $\mu = 1.5$ GeV.

In the PQCD approach the gluon invariant mass l^2 is related to the parton momenta, such that the corresponding factorization formulas involve the convolutions of all three meson distribution amplitudes. Because the nonfactorizable contributions are negligible, we calculate only the magnetic-penguin corrections to the the factorizable amplitudes, which modify only $\mathcal{A}_f^{(t)}$ in Eq. (9):

$$\begin{aligned}
\mathcal{A}^{(t)}_{\pi^+K^0} &\to \mathcal{A}^{(t)}_{\pi^+K^0} - \mathcal{M}^{(g)}_{\pi K} \;, \\
\mathcal{A}^{(t)}_{\pi^0K^+} &\to \mathcal{A}^{(t)}_{\pi^0K^+} - \frac{1}{\sqrt{2}}\mathcal{M}^{(g)}_{\pi K} \;, \\
\mathcal{A}^{(t)}_{\pi^-K^+} &\to \mathcal{A}^{(t)}_{\pi^-K^+} - \mathcal{M}^{(g)}_{\pi K} \;, \\
\mathcal{A}^{(t)}_{\pi^0K^0} &\to \mathcal{A}^{(t)}_{\pi^0K^0} + \frac{1}{\sqrt{2}}\mathcal{M}^{(g)}_{\pi K} \;, \\
\mathcal{A}^{(t)}_{\pi^+\pi^-} &\to \mathcal{A}^{(t)}_{\pi^+\pi^-} - \mathcal{M}^{(g)}_{\pi\pi} \;, \\
\mathcal{A}^{(t)}_{\pi^+\pi^0} &\to \mathcal{A}^{(t)}_{\pi^+\pi^0} \;, \\
\mathcal{A}^{(t)}_{\pi^0\pi^0} &\to \mathcal{A}^{(t)}_{\pi^0\pi^0} - \frac{1}{\sqrt{2}}\mathcal{M}^{(g)}_{\pi\pi} \;. \qquad (38)
\end{aligned}$$

The explicit expressions for the magnetic-penguin amplitudes $\mathcal{M}^{(g)}_{\pi K}$ and $\mathcal{M}^{(g)}_{\pi\pi}$ are referred to Appendix. Since an end-point singularity arises, as the invariant mass l^2 approaches zero, we have employed the k_T factorization theorem, i.e., the PQCD approach in this case.

The effect of the magnetic penguin is just opposite to that of the quark-loop corrections as indicated in Tables III-V: it decreases all the $B \to \pi K, \pi\pi$ branching ratios, except those of the tree-dominated $B^0 \to \pi^\mp\pi^\pm$ and $B^+ \to \pi^\pm\pi^0$ modes, and intends to increase the magnitude of most of the direct CP asymmetries. The mixing-induced CP asymmetry $S_{\pi^0 K_S}$ is stable under the magnetic-penguin correction for the same reason. The magnitude of $S_{\pi\pi}$ decreases due to the smaller penguin pollution. Because the quark-loop corrections are smaller than the magnetic penguin, the pattern of their combined effect is similar to that of the latter. In summary, the above two pieces of NLO corrections reduce the LO penguin amplitudes by about 10% in the $B \to \pi K, \pi\pi$ decays, and the $B \to \pi K$ and $B^0 \to \pi^0\pi^0$ branching ratios by about 20%. The direct CP asymmetries are not altered very much, which are mainly affected by the vertex corrections, as shown by the similarities between the columns +VC and +NLO in Table IV.

IV. THEORETICAL UNCERTAINTY

In this section we explain in detail how to derive the results in Tables III-VI, and discuss their theoretical uncertainty. The PQCD predictions depend on the inputs for the nonperturbative parameters, such as decay constants, distribution amplitudes, and chiral scales for pseudoscalar mesons. For the B meson, the model wave function has been proposed in [21]:

$$\phi_B(x,b) \;=\; N_B x^2(1-x)^2 \exp\left[-\frac{1}{2}\left(\frac{xm_B}{\omega_B}\right)^2 - \frac{\omega_B^2 b^2}{2}\right] \;, \qquad (39)$$

where the Gaussian form was motivated by the oscillator model in [48], and the normalization constant N_B is related to the decay constant f_B through

$$\int_0^1 dx\, \phi_B(x, b=0) \;=\; \frac{f_B}{2\sqrt{2N_c}} \;. \qquad (40)$$

There are certainly other models of the B meson wave function available in the literature (see [49, 50]). It has been confirmed that the model in Eq. (39) and the model derived in [51] with a different functional form lead to similar numerical results for the $B \to \pi$ transition form factor [52].

The twist-2 pion (kaon) distribution amplitude $\phi^A_{\pi(K)}$, and the twist-3 ones $\phi^P_{\pi(K)}$ and $\phi^T_{\pi(K)}$ have been parameterized as

$$\phi^A_{\pi(K)}(x) \;=\; \frac{f_{\pi(K)}}{2\sqrt{2N_c}}\, 6x(1-x)\left[1 + a_1^{\pi(K)} C_1^{3/2}(2x-1) + a_2^{\pi(K)} C_2^{3/2}(2x-1) + a_4^{\pi(K)} C_4^{3/2}(2x-1)\right] \;, \quad (41)$$

$$\phi^P_{\pi(K)}(x) = \frac{f_{\pi(K)}}{2\sqrt{2N_c}}\left[1+\left(30\eta_3-\frac{5}{2}\rho^2_{\pi(K)}\right)C_2^{1/2}(2x-1)\right.$$
$$\left.-3\left\{\eta_3\omega_3+\frac{9}{20}\rho^2_{\pi(K)}(1+6a_2^{\pi(K)})\right\}C_4^{1/2}(2x-1)\right], \quad (42)$$

$$\phi^T_{\pi(K)}(x) = \frac{f_{\pi(K)}}{2\sqrt{2N_c}}(1-2x)\left[1+6\left(5\eta_3-\frac{1}{2}\eta_3\omega_3-\frac{7}{20}\rho^2_{\pi(K)}-\frac{3}{5}\rho^2_{\pi(K)}a_2^{\pi(K)}\right)(1-10x+10x^2)\right], \quad (43)$$

with $a_1^\pi = 0$, the mass ratio $\rho_{\pi(K)} = (m_u + m_{d(s)})/m_{\pi(K)} = m_{\pi(K)}/m_{0\pi(K)}$ and the Gegenbauer polynomials $C_n^\nu(t)$,

$$C_2^{1/2}(t) = \frac{1}{2}\left(3\,t^2-1\right), \; C_4^{1/2}(t) = \frac{1}{8}\left(3-30\,t^2+35\,t^4\right),$$
$$C_1^{3/2}(t) = 3\,t, \qquad C_2^{3/2}(t) = \frac{3}{2}\left(5\,t^2-1\right), \qquad C_4^{3/2}(t) = \frac{15}{8}\left(1-14\,t^2+21\,t^4\right). \quad (44)$$

In the above kaon distribution amplitudes the momentum fraction x is carried by the s quark. For both the pion and kaon, we choose $\eta_3 = 0.015$ and $\omega_3 = -3$ [53]. Because we did not employ the equations of motions for the twist-3 meson distribution amplitudes [25], we are allowed to include the higher Gegenbauer terms, which are in fact important. However, we drop the derivative term with respect to the transverse parton momentum k_T in $\phi^T_{\pi(K)}$. It has been observed that the contribution from this derivative term to the $B \to \pi$ form factor is negligible [54].

In our previous works we adopted the models of the pion and kaon distribution amplitudes derived from QCD sum rules in [53]. Fixing the B meson decay constant $f_B \approx 190$ MeV from lattice QCD (see [55]), the shape parameter of the B meson wave function was determined to be $\omega_B \approx 0.4$ GeV [21] from the $B \to \pi$ form factor $F_+^{B\pi}(0) \approx 0.3$ in light-cone sum rules [56, 57]. The chiral scales were chosen as $m_{0\pi} \approx 1.3$ GeV for the pion and $m_{0K} \approx 1.7$ GeV for the kaon [2]. The renormalization scale μ was set to the off-shellness of the internal particles, consistent with the BLM procedure. The resultant PQCD predictions [2] have been confirmed by the observed $B \to \pi K$ branching ratios and $B^0 \to \pi^\mp K^\pm$ direct CP asymmetry. The consistency indicates not only that the above inputs are reasonable, but that the short-distance QCD dynamics has been described correctly in PQCD.

In this paper we employ the updated models of the pion and kaon distribution amplitudes in [58]. Since the updated Gegenbauer coefficient $a_2^\pi = 0.115$ is smaller than the previous one 0.44 for the twist-2 pion distribution amplitude [53], $F_+^{B\pi}(0)$ reduces compared to that obtained in [24]. To compensate this reduction, we increase the B meson decay constant up to $f_B = 210$ MeV, which is consistent with the recent lattice result [59], in order to maintain the $B \to \pi K$, $\pi\pi$ branching ratios. For the same reason, the penguin annihilation amplitudes, which involve the π-K or π-π time-like form factor, decrease. The magnitude of the resultant direct CP asymmetries of the $B \to \pi K$, $\pi\pi$ decays, which is not compensated by the overall decay constant f_B, then becomes smaller than in [24] as shown in the column LO of Table IV. The smaller $B^0 \to \pi^\mp K^\pm$ direct CP asymmetry is in better agreement with the data, implying that the data could be covered by the theoretical uncertainty at LO of PQCD.

All the above nonperturbative inputs suffer uncertainties, and it is necessary to investigate how these uncertainties propagate into the predictions for nonleptonic B meson decays. Here we shall constrain the shape parameter ω_B and the Gegenbauer coefficients of the twist-2 pion distribution amplitude ϕ_π^A using the experimental error of the semileptonic decay $B \to \pi l\nu$. The sufficient uncertainties will be assigned to the Gegenbauer coefficients of the twist-2 kaon distribution amplitude ϕ_K^A. The other inputs, such as the B meson decay constant, the twist-3 distribution amplitudes, and the chiral scale associated with the pion and the kaon will be fixed. On one hand, the considered sources of theoretical uncertainties have been representative enough. On the other hand, it is impossible to constrain all the inputs with the currently available data.

The spectrum of the semileptonic decay $B \to \pi l\nu$ in the lepton invariant mass q^2 has been measured [60]:

$$\frac{\int_0^8 (d\Gamma/dq^2)dq^2}{\Gamma_{\rm total}} = (0.43 \pm 0.11) \times 10^{-4}, \quad (45)$$

with the total decay rate $\Gamma_{\rm total} = (4.29 \pm 0.04) \times 10^{-13}$ GeV [61]. Assuming that the above error is uniform in the region $0 < q^2 < 8$ GeV^2, we derive the uncertainty Δ of $(d\Gamma/dq^2)|_{q^2=0}$ by solving the equation $8\Delta =$

$0.11 \times 10^{-4}\,\Gamma_{\rm total}$, where we take only the central value of $\Gamma_{\rm total}$ for simplicity. With the allowed range of $|V_{ub}| = (3.67 \pm 0.47) \times 10^{-3}$ [61], Δ is translated into the uncertainty of the $B \to \pi$ form factor,

$$F_+^{B\pi}(0) \;=\; 0.24 \pm 0.05 \;, \tag{46}$$

whose central value comes from our choice of the inputs. Equation (46) is consistent with 0.23 ± 0.04 extracted in [62] from a global fit to the above CLEO data, lattice QCD results of $F_+^{B\pi}(q^2)$, etc. A numerical analysis indicates that $F_+^{B\pi}(0)$ is more sensitive to ω_B than to the Gegenbauer coefficients of ϕ_π^A.

Therefore, we propose

1. the shape parameters for the distribution amplitudes,

$$\begin{aligned} &\omega_B \;=\; (0.40 \pm 0.04)\;{\rm GeV}\;, \quad a_2^\pi \;=\; 0.115 \pm 0.115\;, \quad a_4^\pi \;=\; -0.015\;, \\ &a_1^K \;=\; 0.17 \pm 0.17\;, \quad a_2^K \;=\; 0.115 \pm 0.115\;, \quad a_4^K \;=\; -0.015\;, \end{aligned} \tag{47}$$

   that is, the Gegenbauer coefficients can vary by 100%. We do not consider the uncertainty from the coefficients a_4^π and a_4^K, to which our predictions are insensitive. Note that the first Gegenbauer coefficients $a_1^K \approx 0.10 \pm 0.12$ and $a_1^K \approx 0.05 \pm 0.02$ have been found to be smaller in [63] and [64], respectively. A hint on the effect from the evolution of the meson distribution amplitudes from $1/b$ down to the cutoff μ_0 (see Sec. III) can also be obtained through the above variation of the Gegenbauer coefficients.

2. the CKM matrix elements,

$$\begin{aligned} &V_{ud} \;=\; 0.9734\;, \quad V_{us} \;=\; 0.2200\;, \quad |V_{ub}| \;=\; (3.67 \pm 0.47) \times 10^{-3}\;, \\ &V_{cd} \;=\; -0.224\;, \quad V_{cs} \;=\; 0.996\;, \quad V_{cb} \;=\; 0.0413\;, \end{aligned} \tag{48}$$

   where we consider only the representative source of theoretical uncertainties from $|V_{ub}|$ [61]. This source is essential for estimating the uncertainty of the predicted direct CP asymmetries. $V_{cb} = (41.3 \pm 1.5) \times 10^{-3}$ [61] has a smaller uncertainty, and the other matrix elements have been known more precisely. The unitarity condition $V_{tb}V_{ts(d)}^* = -V_{ub}V_{us(d)}^* - V_{cb}V_{cs(d)}^*$ is then employed as evaluating the penguin contributions.

3. the weak phases,

$$\phi_1 \;=\; 21.6^\circ\;, \quad \phi_3 \;=\; (70 \pm 30)^\circ\;, \tag{49}$$

   where the range of the well-measured ϕ_1 with $\sin(2\phi_1) = 0.685 \pm 0.032$ [65] has been neglected, and the range of ϕ_3 is hinted by the determinations [65, 66],

$$\begin{aligned} \phi_3 \;=\; & 68^{+14}_{-15} \pm 13 \pm 11 \;\; ({\rm Belle, Dalitz})\;, \\ & 70 \pm 31^{+12+14}_{-10-11} \;\; ({\rm BaBar, Dalitz})\;, \\ & 63^{+15}_{-13} \;\; ({\rm CKMfitter})\;, \\ & 64 \pm 18 \;\; ({\rm UTfit})\;. \end{aligned} \tag{50}$$

We fix the other parameters, such as the meson decay constants $f_B = 210$ MeV, $f_K = 160$ MeV, $f_\pi = 130$ MeV, the meson masses $m_B = 5.28$ GeV, $m_K = 0.49$ GeV, $m_\pi = 0.14$ GeV, the charm quark mass $m_c = 1.5$ GeV, and the B meson lifetimes $\tau_{B^0} = 1.528 \times 10^{-12}$ sec, $\tau_{B^\pm} = 1.643 \times 10^{-12}$ sec [1]. We also fix the chiral scales $m_{0\pi} = 1.3$ GeV and $m_{0K} = 1.7$ GeV, where the value of $m_{0\pi}$ (m_{0K}) is close to that (larger than 1.25 ± 0.15 GeV) obtained in the recent sum-rule analysis [67]. The resultant $B \to \pi, K$ transition form factors,

$$F_+^{B\pi}(0) \;=\; 0.24^{+0.05}_{-0.04}\;, \quad F_+^{BK}(0) \;=\; 0.36^{+0.09}_{-0.07}\;, \tag{51}$$

respect Eq. (46) from the measurement, and are consistent with the estimation from light-cone sum rules [64]. If further including the variation of m_{0K} as a source of theoretical uncertainties, we just enlarge the range of the $B \to \pi K$ branching ratios, but not of the other quantities. We have tested the dependence of our predictions on the cutoff μ_0, which is found to be weak.

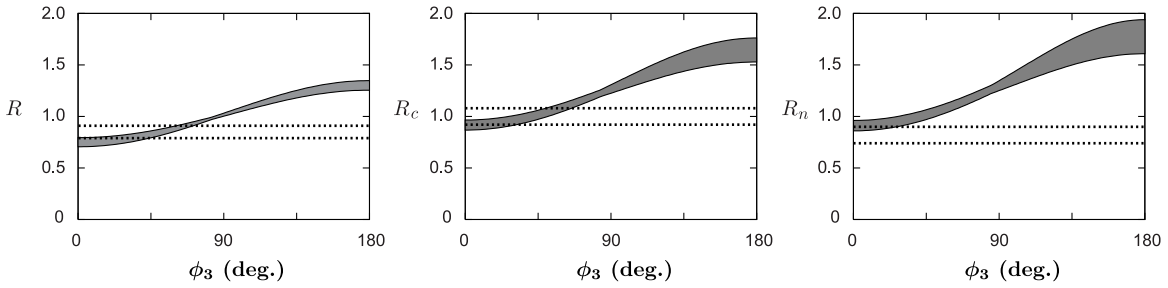

FIG. 4: Dependence of R, R_c, and R_n on ϕ_3 from NLO PQCD with the bands representing the theoretical uncertainty. The two dashed lines represent 1σ bounds from the data.

The above inputs lead to Tables III-VI, where the theoretical uncertainties are displayed only in the columns +NLO. The errors (not) in the parentheses represent those from (all sources) the first source of uncertainties. It indicates that the nonperturbative inputs, i.e., the first source, contribute to the theoretical uncertainties more dominantly in the $B \to \pi K$ decays than in the $B \to \pi\pi$ decays, because the former depend on the less controllable parameters associated with the kaon. We also observe that $A_{CP}(B^0 \to \pi^\mp K^\pm)$ and $A_{CP}(B^\pm \to \pi^0 K^\pm)$ always increase or decrease simultaneously, when varying the nonperturbative inputs. Hence, the $B \to \pi K$ puzzle can not be resolved by tuning these parameters. After including the uncertainties, the predicted $B^0 \to \pi^0\pi^0$ branching ratio and mixing-induced CP asymmetry $S_{\pi^0 K_S}$ are still far from the data.

A more transparent comparison between the predictions and the data is made by considering the ratios of the branching ratios. The following three ratios of the $B \to \pi K$ branching ratios have been widely studied in the literature,

$$\begin{aligned} R &= \frac{B(B^0 \to \pi^\mp K^\pm)}{B(B^\pm \to \pi^\pm K^0)} \frac{\tau_{B^+}}{\tau_{B^0}} = 0.85 \pm 0.06 \,, \\ R_c &= 2\,\frac{B(B^\pm \to \pi^0 K^\pm)}{B(B^\pm \to \pi^\pm K^0)} = 1.00 \pm 0.08 \,, \\ R_n &= \frac{1}{2}\,\frac{B(B^0 \to \pi^\mp K^\pm)}{B(B^0 \to \pi^0 K^0)} = 0.82 \pm 0.08 \,, \end{aligned} \tag{52}$$

whose values are quoted from [1]. We have confirmed that these ratios depend on the nonperturbative inputs weakly. Therefore, their deviation from the standard-model predictions could reveal a signal of new physics, such as a large electroweak penguin amplitude. Table III shows that for $\phi_3 = 70°$, the ratio R increases slightly from 0.90 to 0.92, when the NLO Wilson coefficients are adopted, beyond which the various NLO corrections do not change R much. The ratio R_c (R_n) decreases from 1.20 (1.25) to 1.14 (1.14), when the NLO Wilson coefficients are adopted, and settles down at this value as indicated by the column +NLO. The different types of NLO corrections cause only small fluctuations. Comparing the columns LO and +NLO, the consistency between the PQCD predictions and the data has been improved.

Varying the weak phase ϕ_3 and the inputs, we find that the PQCD predictions for R and R_n are in good agreement with the data in Eq. (52), which is obvious from Fig. 4. However, the predictions for R_n exhibit a tendency of overshooting the data, which is attributed to the smaller PQCD results for the $B^0 \to \pi^0 K^0$ branching ratio. A smaller Gegenbauer coefficient a_2^π of ϕ_π^A enhances R_n. That is, when using the updated pion distribution amplitudes from [58], the consistency of the predictions for R_n with the data deteriorates. A smaller ω_B enhances R_n. This is the reason we do not lower ω_B in order to compensate the reduction from the smaller a_2^π. Note that m_{0K} has an effect on the electroweak penguin amplitude, i.e., on the $B^0 \to \pi^0 K^0$ branching ratio. Hence, we have also studied the dependence of R_n on the chiral scale m_{0K}. A smaller m_0^K indeed reduces R_n, but does not help much: choosing $m_{0K} = 1.3$ GeV causes only few percent reduction of R_n. It has been known that the $B^0 \to \pi^0 K^0$ branching ratio can be significantly increased by rotating the electroweak penguin amplitude P'_{ew} away from the penguin amplitude P' (their values in Table V are roughly parallel to each other). Therefore, we can not rule out the possibility that P'_{ew} acquires an additional phase from new physics effects [9, 68, 69]. However, our theoretical uncertainty is representative, and the actual uncertainty could be larger, such that the discrepancy is not serious at this moment. We do not discuss the ratios relevant to the $B \to \pi\pi$

decays, because the PQCD predictions for the $B^0 \to \pi^0\pi^0$ branching ratio are currently far below the measured values.

V. CONCLUSION

The LO PQCD has correctly predicted the direct CP asymmetry $A_{CP}(B^0 \to \pi^\mp K^\pm)$, but failed to explain another one $A_{CP}(B^\pm \to \pi^0 K^\pm)$ [2]. Phenomenologically, the substantial difference between $A_{CP}(B^\pm \to \pi^0 K^\pm)$ and $A_{CP}(B^0 \to \pi^\mp K^\pm)$ has led to the conjecture of new physics [7, 9]. However, the difference can also be attributed to a large color-suppressed tree amplitude C' as pointed out in [13]. Theoretically, an examination of NLO effects is always demanded for a systematic approach like PQCD. Since C' itself is a subdominant contribution, it is easily affected by subleading corrections. Hence, before claiming a new physics signal in the $B \to \pi K$ data, one should at least check whether the NLO effects could enhance C' sufficiently. This is one of our motivations to perform the NLO calculation in PQCD for the $B \to \pi K$, $\pi\pi$ decays here. Another motivation comes from the mixing-induced CP asymmetries in the penguin-dominated modes, some of which also depend on the color-suppressed tree amplitudes. To estimate the deviation of $S_{\pi^0 K_S}$ from $S_{c\bar{c}s}$ within the standard model, one must compute C' reliably.

In this paper we have calculated the NLO corrections to the $B \to \pi K$, $\pi\pi$ decays from the vertex corrections, the quark loops, and the magnetic penguin in the PQCD approach. The results for the branching ratios and CP asymmetries in the NDR scheme have been presented in Tables III-VI, and discussed in Sec. III. It has been shown that the corrections from the quark loops and from the magnetic penguin come with opposite signs, and sum to about 10% of the LO penguin amplitudes. Their effect is to reduce the $B \to \pi K$ branching ratios, to which the penguin contribution is dominant, by about 20%. They have a minor influence on the $B \to \pi\pi$ branching ratios, and CP asymmetries. The vertex corrections play an important role in modifying direct CP asymmetries, especially those of the $B^\pm \to \pi^0 K^\pm$, $B^0 \to \pi^0 K^0$, and $B^0 \to \pi^0\pi^0$ modes, by increasing the color-suppressed tree amplitudes few times. The larger color-suppressed tree amplitude leads to nearly vanishing $A_{CP}(B^\pm \to \pi^0 K^\pm)$, resolving the $B \to \pi K$ puzzle within the standard model. Our analysis has also confirmed that the NLO corrections are under control in PQCD.

The NLO corrections, though increasing the color-suppressed tree amplitudes significantly, are not enough to enhance the $B^0 \to \pi^0\pi^0$ branching ratio to the measured value. A much larger amplitude ratio $|C/T| \sim 0.8$ must be obtained in order to resolve this puzzle [13]. Nevertheless, the NLO corrections do improve the consistency of our predictions with the data: the predicted $B^0 \to \pi^\pm\pi^\mp$ ($B^0 \to \pi^0\pi^0$) branching ratio decreases (increases). Viewing the consistency of the PQCD predictions with the tiny measured $B^0 \to K^0\overline{K}^0$ and $B^0 \to \rho^0\rho^0$ branching ratios, we think that our NLO results for the $B \to \pi\pi$ decays are reasonable. In SCET [30], the large $|C/T|$ comes from a fit to the data, instead of from an explicit evaluation of the amplitudes. The amplitude C was indeed found to be increased in SCET by the NLO jet function (the short-distance coefficient from matching $\mathrm{SCET_I}$ to $\mathrm{SCET_{II}}$) [70], if the parameter set "S4" in QCDF [25] was adopted. The large measured $B^0 \to \pi^0\pi^0$ branching ratio was then explained. However, we emphasize again that the same analysis should be applied to the $B \to \rho\rho$ decays for a check. Hence, the $B \to \pi\pi$ puzzle still requires more investigation.

The tendency of overshooting the observed ratio R_n has implied a possible new-physics phase associated with the electroweak penguin amplitude P'_{ew}. This additional phase can render P'_{ew} orthogonal to the penguin amplitude, and enhance the $B^0 \to \pi^0 K^0$ branching ratio. We have also computed the deviation $\Delta S_{\pi^0 K_S}$ of the mixing-induced CP asymmetry, and found that the NLO effects push it toward the even larger positive value. Therefore, it is difficult to understand the observed negative deviation without physics beyond the standard model.

We thank T. Browder, H.Y. Cheng, C.K. Chua, W.S. Hou, Y.Y. Keum, M. Nagashima, A. Soddu, and A. Soni for useful discussions. This work was supported by the National Science Council of R.O.C. under Grant No. NSC-94-2112-M-001-001, and by the Grants-in-aid from the Ministry of Education, Culture, Sports, Science and Technology, Japan under Grant No. 14046201. HNL acknowledges the hospitality of Department of Physics, Hawaii University, where this work was initiated.

APPENDIX: FACTORIZATION FORMULAS

We first define the kinematics for the $B \to M_2 M_3$ decay, where M_2 (M_3) denotes the light pseudo-scalar meson involved in the B meson transition (emitted from the weak vertex). In the rest frame of the B meson, the B (M_2, M_3) meson momentum P_1 (P_2, P_3), and the corresponding spectator quark momentum k_1 (k_2, k_3) are taken, in the light-cone coordinates, as

$$\begin{aligned} P_1 &= \frac{m_B}{\sqrt{2}}(1,1,\mathbf{0}_T)\,, & k_1 &= (0, x_1 P_1^-, \mathbf{k}_{1T})\,, \\ P_2 &= \frac{m_B}{\sqrt{2}}(1,0,\mathbf{0}_T)\,, & k_2 &= (x_2 P_2^+, 0, \mathbf{k}_{2T})\,, \\ P_3 &= \frac{m_B}{\sqrt{2}}(0,1,\mathbf{0}_T)\,, & k_3 &= (0, x_3 P_3^-, \mathbf{k}_{3T})\,, \end{aligned} \tag{A.1}$$

where the light meson masses have been neglected. We also define the ratio $r_2 = m_{02}/m_B$ ($r_3 = m_{03}/m_B$) associated with the meson M_2 (M_3), m_{02} (m_{03}) being the chiral scale.

The factorization formulas for the $B \to M_2 M_3$ decay amplitudes appearing in Tables I and II are collected below:

$$\begin{aligned} F_{e4}(a) &= 16\pi C_F m_B^2 \int_0^1 dx_1 dx_2 \int_0^\infty b_1 db_1\, b_2 db_2\, \phi_B(x_1,b_1) \\ &\times\Big\{ \left[(1+x_2)\phi_2^A(\overline{x_2}) + r_2(1-2x_2)\left(\phi_2^P(\overline{x_2}) - \phi_2^T(\overline{x_2})\right)\right] E_e(t) h_e(A,B,b_1,b_2,x_2) \\ &\quad + 2r_2\phi_2^P(\overline{x_2}) E_e(t') h_e(A',B',b_2,b_1,x_1)\Big\}\,, \end{aligned} \tag{A.2}$$

$$\begin{aligned} F_{e6}(a) &= 32\pi C_F m_B^2 \int_0^1 dx_1 dx_2 \int_0^\infty b_1 db_1\, b_2 db_2\, \phi_B(x_1,b_1) \\ &\times\Big\{ r_3\left[\phi_2^A(\overline{x_2}) + r_2 x_2\left(\phi_2^P(\overline{x_2}) + \phi_2^T(\overline{x_2})\right) + 2r_2\phi_2^P(\overline{x_2})\right] E_e(t) h_e(A,B,b_1,b_2,x_2) \\ &\quad + 2r_2 r_3 \phi_2^P(\overline{x_2}) E_e(t') h_e(A',B',b_2,b_1,x_1)\Big\}\,, \end{aligned} \tag{A.3}$$

$$\begin{aligned} F_{a4}(a) &= 16\pi C_F m_B^2 \int_0^1 dx_2 dx_3 \int_0^\infty b_2 db_2\, b_3 db_3 \\ &\times\Big\{ \left[x_3\phi_2^A(\overline{x_2})\phi_3^A(\overline{x_3}) + 2r_2 r_3 \phi_2^P(\overline{x_2})\left\{\left(\phi_3^P(\overline{x_3}) + \phi_3^T(\overline{x_3})\right) + x_3\left(\phi_3^P(\overline{x_3}) - \phi_3^T(\overline{x_3})\right)\right\}\right] \\ &\quad \times E_a(t) h_e(A,B,b_2,b_3,x_3) \\ &\quad - \left[(1-x_2)\phi_2^A(\overline{x_2})\phi_3^A(\overline{x_3}) - 2r_2 r_3\left\{-2\phi_2^P(\overline{x_2}) + x_2\left(\phi_2^P(\overline{x_2}) + \phi_2^T(\overline{x_2})\right)\right\}\phi_3^P(\overline{x_3})\right] \\ &\quad \times E_a(t') h_e(A',B',b_3,b_2,x_2)\Big\}\,, \end{aligned} \tag{A.4}$$

$$\begin{aligned} F_{a6}(a) &= 32\pi C_F m_B^2 \int_0^1 dx_2 dx_3 \int_0^\infty b_2 db_2\, b_3 db_3 \\ &\times\Big\{ \left[2r_2\phi_2^P(\overline{x_2})\phi_3^A(\overline{x_3}) + r_3 x_3 \phi_2^A(\overline{x_2})\left(\phi_3^P(\overline{x_3}) + \phi_3^T(\overline{x_3})\right)\right] E_a(t) h_e(A,B,b_2,b_3,x_3) \\ &\quad + \left[r_2(1-x_2)\left(\phi_2^P(\overline{x_2}) - \phi_2^T(\overline{x_2})\right)\phi_3^A(\overline{x_3}) + 2r_3\phi_2^A(\overline{x_2})\phi_3^P(\overline{x_3})\right] \\ &\quad \times E_a(t') h_e(A',B',b_3,b_2,x_2)\Big\}\,, \end{aligned} \tag{A.5}$$

$$\begin{aligned} \mathcal{M}_{e4}(a') &= 32\pi C_F \frac{\sqrt{2N_c}}{N_c} m_B^2 \int_0^1 dx_1 dx_2 dx_3 \int_0^\infty b_1 db_1\, b_3 db_3\, \phi_B(x_1,b_1)\phi_3^A(\overline{x_3}) \\ &\times\Big\{ \left[(1-x_3)\phi_2^A(\overline{x_2}) - r_2 x_2\left(\phi_K^P(\overline{x_2}) + \phi_K^T(\overline{x_2})\right)\right] E_e'(t) h_n(A,B,b_1,b_3) \end{aligned}$$

	A	B	A'	B'
$F_{e4,e6}$	$\sqrt{x_2}m_B$	$\sqrt{x_1x_2}m_B$	$\sqrt{x_1}m_B$	$\sqrt{x_1x_2}m_B$
$\mathcal{M}_{e4,e5,e6}$	$i\sqrt{x_2(\overline{x_3}-x_1)}m_B$	$\sqrt{x_1x_2}m_B$	$\sqrt{x_2(x_1-x_3)}m_B$	$\sqrt{x_1x_2}m_B$
$F_{a4,a6}$	$i\sqrt{x_3}m_B$	$i\sqrt{\overline{x_2}x_3}m_B$	$i\sqrt{\overline{x_2}}m_B$	$i\sqrt{\overline{x_2}x_3}m_B$
$\mathcal{M}_{a4,a5,a6}$	$\sqrt{(x_1-x_3)\overline{x_2}}m_B$	$i\sqrt{\overline{x_2}x_3}m_B$	$\sqrt{1-x_2(\overline{x_3}-x_1)}m_B$	$i\sqrt{\overline{x_2}x_3}m_B$

TABLE VIII: The invariant masses A, B, A', and B' in the hard kernels.

$$+\left[-(x_2+x_3)\phi_2^A(\overline{x_2})+r_2x_2\left(\phi_2^P(\overline{x_2})-\phi_2^T(\overline{x_2})\right)\right]E_e'(t')h_n(A',B',b_1,b_3)\Bigg\}\,, \tag{A.6}$$

$$\begin{aligned}
\mathcal{M}_{e6}(a') &= 32\pi C_F\frac{\sqrt{2N_c}}{N_c}m_B^2\,r_3\int_0^1 dx_1dx_2dx_3\int_0^\infty b_1db_1\,b_3db_3\,\phi_B(x_1,b_1)\\
&\times\Bigg\{\left[(1-x_3)\phi_2^A(\overline{x_2})\left(\phi_3^P(\overline{x_3})-\phi_3^T(\overline{x_3})\right)\right.\\
&\quad+r_2(1-x_3)\left(\phi_2^P(\overline{x_2})+\phi_2^T(\overline{x_2})\right)\left(\phi_3^P(\overline{x_3})-\phi_3^T(\overline{x_3})\right)\\
&\quad\left.+r_2x_2\left(\phi_2^P(\overline{x_2})-\phi_2^T(\overline{x_2})\right)\left(\phi_3^P(\overline{x_3})+\phi_3^T(\overline{x_3})\right)\right]E_e'(t)h_n(A,B,b_1,b_3)\\
&-\left[x_3\phi_2^A(\overline{x_2})\left(\phi_3^P(\overline{x_3})+\phi_3^T(\overline{x_3})\right)+r_2x_3\left(\phi_2^P(\overline{x_2})+\phi_2^T(\overline{x_2})\right)\left(\phi_3^P(\overline{x_3})+\phi_3^T(\overline{x_3})\right)\right.\\
&\quad\left.+r_2x_2\left(\phi_2^P(\overline{x_2})-\phi_2^T(\overline{x_2})\right)\left(\phi_3^P(\overline{x_3})-\phi_3^T(\overline{x_3})\right)\right]E_e'(t')h_n(A',B',b_1,b_3)\Bigg\}\,,
\end{aligned} \tag{A.7}$$

$$\begin{aligned}
\mathcal{M}_{a4}(a') &= 32\pi C_F\frac{\sqrt{2N_c}}{N_c}m_B^2\int_0^1 dx_1dx_2dx_3\int_0^\infty b_1db_1\,b_3db_3\,\phi_B(x_1,b_1)\\
&\times\Bigg\{\left[(1-x_2)\phi_2^A(\overline{x_2})\phi_3^A(\overline{x_3})+r_2r_3\left\{(1-x_2)\left(\phi_2^P(\overline{x_2})+\phi_2^T(\overline{x_2})\right)\left(\phi_3^P(\overline{x_3})-\phi_3^T(\overline{x_3})\right)\right.\right.\\
&\quad\left.\left.+x_3\left(\phi_2^P(\overline{x_2})-\phi_2^T(\overline{x_2})\right)\left(\phi_3^P(\overline{x_3})+\phi_3^T(\overline{x_3})\right)\right\}\right]E_a'(t)h_n(A,B,b_3,b_1)\\
&-\left[x_3\phi_2^A(\overline{x_2})\phi_3^A(\overline{x_3})+r_2r_3\left\{4\phi_2^P(\overline{x_2})\phi_3^P(\overline{x_3})\right.\right.\\
&\quad-(1-x_3)\left(\phi_2^P(\overline{x_2})+\phi_2^T(\overline{x_2})\right)\left(\phi_3^P(\overline{x_3})-\phi_3^T(\overline{x_3})\right)\\
&\quad\left.\left.-x_2\left(\phi_2^P(\overline{x_2})-\phi_2^T(\overline{x_2})\right)\left(\phi_3^P(\overline{x_3})+\phi_3^T(\overline{x_3})\right)\right\}\right]E_a'(t')h_n(A',B',b_3,b_1)\Bigg\}\,,
\end{aligned} \tag{A.8}$$

$$\begin{aligned}
\mathcal{M}_{a6}(a') &= 32\pi C_F\frac{\sqrt{2N_c}}{N_c}m_B^2\int_0^1 dx_1dx_2dx_3\int_0^\infty b_1db_1\,b_3db_3\,\phi_B(x_1,b_1)\\
&\times\Bigg\{\Big[-r_2(1-x_2)\left(\phi_2^P(\overline{x_2})+\phi_2^T(\overline{x_2})\right)\phi_3^A(\overline{x_3})\\
&\quad+r_3x_3\phi_2^A(\overline{x_2})\left(\phi_3^P(\overline{x_3})-\phi_3^T(\overline{x_3})\right)\Big]E_a'(t)h_n(A,B,b_3,b_1)\\
&-\Big[r_2(1+x_2)\left(\phi_2^P(\overline{x_2})+\phi_2^T(\overline{x_2})\right)\phi_3^A(\overline{x_3})\\
&\quad+r_3(-2+x_3)\phi_2^A(\overline{x_2})\left(\phi_3^P(\overline{x_3})-\phi_3^T(\overline{x_3})\right)\Big]E_a'(t')h_n(A',B',b_3,b_1)\Bigg\}\,,
\end{aligned} \tag{A.9}$$

where we have adopted the notations $\overline{x_2}\equiv 1-x_2$ and $\overline{x_3}\equiv 1-x_3$, and ignored the mass difference between m_B and m_b. F_{eKi} and $\mathcal{M}_{eKi}$ are obtained by choosing M_2 (M_3) to be the kaon (pion) in F_{ei} and $\mathcal{M}_{ei}$, respectively.

The invariant masses A, B, A', and B' of the virtual quarks and gluons involved in the above hard kernels are functions of x_1, x_2 and x_3, as in Table VIII. The hard scales are chosen as

$$\begin{aligned}
t &= \max(\sqrt{|A^2|},\,\sqrt{|B^2|},\,1/b_i)\,,\\
t' &= \max(\sqrt{|A'^2|},\,\sqrt{|B'^2|},\,1/b_i)\,,
\end{aligned} \tag{A.10}$$

with the index $i = 1, 2$ for $F_{e4,e6}$, $i = 2, 3$ for $F_{a4,a6}$, and $i = 1, 3$ for the nonfactorizable amplitudes.

The evolution factors $E_e^{(\prime)}$ and $E_a^{(\prime)}$ are given by

$$\begin{aligned} E_e(t) &= \alpha_s(t)\, a(t) \exp[-S_B(t) - S_2(t)] \,, \\ E_a(t) &= \alpha_s(t)\, a(t) \exp[-S_2(t) - S_3(t)] \,, \\ E'_e(t) &= \alpha_s(t)\, a'(t) \exp[-S_B(t) - S_2(t) - S_3(t)]|_{b_2=b_1} \,, \\ E'_a(t) &= \alpha_s(t)\, a'(t) \exp[-S_B(t) - S_2(t) - S_3(t)]|_{b_2=b_3} \,, \end{aligned} \tag{A.11}$$

where $a^{(\prime)}$ represent the combination of the Wilson coefficients appearing in Tables I and II. The Sudakov exponents associated with the various mesons are written as

$$S_B(t) = \exp\left[-s(x_1 P_1^+, b_1) - \frac{5}{3}\int_{1/b_1}^{t} \frac{d\bar{\mu}}{\bar{\mu}} \gamma_q(\alpha_s(\bar{\mu}))\right] \,, \tag{A.12}$$

$$S_2(t) = \exp\left[-s(x_2 P_2^+, b_2) - s((1-x_2) P_2^+, b_2) - 2\int_{1/b_2}^{t} \frac{d\bar{\mu}}{\bar{\mu}} \gamma_q(\alpha_s(\bar{\mu}))\right] \,, \tag{A.13}$$

with the quark anomalous dimension $\gamma_q = -\alpha_s/\pi$. The formula for the exponential S_3 is the same as S_2 but with the kinematic variables of meson 2 being replaced by those of meson 3. The explicit expression of the exponent s can be found in [20, 71, 72]. The variable b_1, conjugate to the parton transverse momentum k_{1T}, represents the transverse extent of the B meson. The transverse extents b_2 and b_3 have the similar meaning for mesons 2 and 3, respectively. For the running coupling constant $\alpha_s(\bar{\mu})$, we employ the one-loop expression, and the QCD scale $\Lambda^{(4)}_{\rm QCD} = 0.250$ GeV. The Sudakov exponential decreases fast in the large b region, such that the long-distance contribution to the decay amplitude is suppressed.

The hard functions are written as

$$\begin{aligned} h_e(A, B, b_1, b_2, x_i) &= [\theta(b_1 - b_2) K_0(Ab_1) I_0(Ab_2) \\ &\quad + \theta(b_2 - b_1) K_0(Ab_2) I_0(Ab_1)] K_0(Bb_1)\ S_t(x_i) \,, \end{aligned} \tag{A.14}$$

$$\begin{aligned} h_n(A, B, b_1, b_3) &= K_0(Ab_3) [\theta(b_1 - b_3) K_0(Bb_1) I_0(Bb_3) \\ &\quad + \theta(b_3 - b_1) K_0(Bb_3) I_0(Bb_1)] \,, \end{aligned} \tag{A.15}$$

where S_t resums the threshold logarithm $\ln^2 x$ appearing the hard kernels to all orders. It has been parameterized as [73]

$$S_t(x) = \frac{2^{1+2c}\,\Gamma(3/2 + c)}{\sqrt{\pi}\,\Gamma(1+c)} [x(1-x)]^c \,, \tag{A.16}$$

with $c = 0.3$.

The factorization formulas for $\mathcal{M}^{(q)}_{\pi K}$, $q = u, c, t$, involve the convolutions of all three meson distribution amplitudes:

$$\begin{aligned} \mathcal{M}^{(q)}_{\pi K} &= -16 m_B^2 \frac{C_F^2}{\sqrt{2N_c}} \int_0^1 dx_1 dx_2 dx_3 \int_0^\infty b_1 db_1 b_2 db_2 \phi_B(x_1, b_1) \\ &\quad \times \Big\{ \left[(1+x_2)\phi_\pi^A(\overline{x_2})\phi_K^A(\overline{x_3}) + r_\pi(1-2x_2)\left(\phi_\pi^P(\overline{x_2}) - \phi_\pi^T(\overline{x_2})\right)\phi_K^A(\overline{x_3})\right. \\ &\qquad \left. + 2r_K \phi_\pi^A(\overline{x_2})\phi_K^P(\overline{x_3}) + 2r_\pi r_K\left((2+x_2)\phi_\pi^P(\overline{x_2}) + x_2\phi_\pi^T(\overline{x_2})\right)\phi_K^P(\overline{x_3})\right] \\ &\qquad \times E^{(q)}(t_q, l^2) h_e(A, B, b_1, b_2, x_2) \\ &\quad + \left[2r_\pi \phi_\pi^P(\overline{x_2})\phi_K^A(\overline{x_3}) + 4r_\pi r_K \phi_\pi^P(\overline{x_2})\phi_K^P(\overline{x_3})\right] \\ &\qquad \times E^{(q)}(t'_q, l'^2) h_e(A', B', b_2, b_1, x_1)\Big\} \,, \end{aligned} \tag{A.17}$$

with the evolution factor,

$$E^{(q)}(t, l^2) = [\alpha_s(t)]^2\, C^{(q)}(t, l^2) \exp\left[-S_B(t) - S_\pi(t)\right] \,. \tag{A.18}$$

The hard scales are chosen as

$$
\begin{aligned}
t_q &= \max\left(\sqrt{|A^2|},\, \sqrt{|B^2|},\, \sqrt{\overline{x_2}x_3}m_B,\, 1/b_i\right) , \\
t'_q &= \max\left(\sqrt{|A'^2|},\, \sqrt{|B'^2|},\, \sqrt{|x_3-x_1|}m_B,\, 1/b_i\right) ,
\end{aligned} \tag{A.19}
$$

with the index $i = 1, 2$. The additional scales $\sqrt{\overline{x_2}x_3}m_B$ and $\sqrt{|x_3 - x_1|}m_B$, compared to those appearing in Eq. (A.10), come from the gluon invariant masses $l^2 = (1-x_2)x_3m_B^2$ and $l'^2 = (x_3-x_1)m_B^2$ in Figs. 2(a) and 2(b), respectively. The formulas for $\mathcal{M}_{\pi\pi}^{(u,c,t)}$ are derived from Eq. (A.17) by substituting the mass ratio r_π for r_K, and the distribution amplitudes ϕ_π^A and ϕ_π^P for ϕ_K^A and ϕ_K^P, respectively.

The magnetic-penguin amplitude is written, for the $B \to \pi K$ modes, as [74]

$$
\begin{aligned}
\mathcal{M}_{\pi K}^{(g)} &= 16m_B^4 \frac{C_F^2}{\sqrt{2N_c}} \int_0^1 dx_1 dx_2 dx_3 \int_0^\infty b_1 db_1\, b_2 db_2\, b_3 db_3\, \phi_B(x_1, b_1) \\
&\times \Big\{ \big[-(1-x_2)\left\{ 2\phi_\pi^A(\overline{x_2}) + r_\pi\left(3\phi_\pi^P(\overline{x_2}) - \phi_\pi^T(\overline{x_2})\right)\right. \\
&\quad \left. + r_\pi x_2\left(\phi_\pi^P(\overline{x_2}) + \phi_\pi^T(\overline{x_2})\right)\right\}\phi_K(\overline{x_3}) \\
&\quad - r_K(1+x_2)x_3\phi_\pi^A(\overline{x_2})\left(3\phi_K^P(\overline{x_3}) + \phi_K^T(\overline{x_3})\right) \\
&\quad - r_K r_\pi(1-x_2)\left(\phi_\pi^P(\overline{x_2}) + \phi_\pi^T(\overline{x_2})\right)\left(3\phi_K^P(\overline{x_3}) - \phi_K^T(\overline{x_3})\right) \\
&\quad - r_K r_\pi x_3(1-2x_2)\left(\phi_\pi^P(\overline{x_2}) - \phi_\pi^T(\overline{x_2})\right)\left(3\phi_K^P(\overline{x_3}) + \phi_K^T(\overline{x_3})\right)\big] \\
&\quad \times E_g(t_q) h_g(A, B, C, b_1, b_2, b_3, x_2) \\
&- \left[4r_\pi\phi_\pi^P(\overline{x_2})\phi_K(\overline{x_3}) + 2r_K r_\pi x_3\phi_\pi^P(\overline{x_2})\left(3\phi_K^P(\overline{x_3}) + \phi_K^T(\overline{x_3})\right)\right] \\
&\quad \times E_g(t'_q) h_g(A', B', C', b_2, b_1, b_3, x_1)\Big\} ,
\end{aligned} \tag{A.20}
$$

with the evolution factor $E_g(t)$,

$$
E_g(t) = [\alpha_s(t)]^2 C_{8g}^{\rm eff}(t) \exp[-S_B(t) - S_K(t) - S_\pi(t)] . \tag{A.21}
$$

Since the terms proportional to $r_K r_\pi$ develop the end-point singularities as the invariant mass of the gluon from O_{8g} vanishes ($x_3 \to 0$), we have kept the transverse momentum k_{3T}. This is the reason the Sudakov factor associated with the kaon appears. The hard function is given by

$$
\begin{aligned}
&h_g(A, B, C, b_1, b_2, b_3, x_i) \\
&= -S_t(x_i)\, K_0\left(Bb_1\right) K_0\left(Cb_3\right) \int_0^{\frac{\pi}{2}} d\theta\, \tan\theta J_0\left(Ab_1\tan\theta\right) J_0\left(Ab_2\tan\theta\right) J_0\left(Ab_3\tan\theta\right) ,
\end{aligned} \tag{A.22}
$$

with the virtual quark and gluon invariant masses,

$$
\begin{aligned}
&A = \sqrt{x_2}m_B , \quad B = B' = \sqrt{x_1x_2}m_B , \quad C = i\sqrt{(1-x_2)x_3}m_B , \\
&A' = \sqrt{x_1}m_B , \quad C' = \sqrt{x_1 - x_3}m_B .
\end{aligned} \tag{A.23}
$$

The hard scales $t_q^{(\prime)}$ are the same as in Eq. (A.19) with the index $i = 1, 2, 3$.

At last, we present the factorization formula for the nonfactorizable amplitude $\mathcal{M}_{e4}$ with the parton transverse degrees of freedom in the kaon being neglected. This formula is employed to justify the approximate equality of an amplitude without the end-point singularity evaluated in collinear and k_T factorization theorems. Dropping the parton transverse momentum k_{3T}, the corresponding change is to remove the factor m_B^2 in Eq. (A.6) and the integration $\int b_3 db_3$. We also replace the hard functions by [75]

$$
h_n(A^{(\prime)}, B^{(\prime)}, b_1, b_3) \to \frac{m_B^2}{B^{(\prime)2} - A^{(\prime)2}} \begin{pmatrix} K_0\left(A^{(\prime)}b_1\right) - K_0\left(B^{(\prime)}b_1\right) & \text{for } A^{(\prime)2} \geq 0 \\ \frac{i\pi}{2}H_0^{(1)}\left(\sqrt{|A^{(\prime)2}|}b_1\right) - K_0\left(B^{(\prime)}b_1\right) & \text{for } A^{(\prime)2} < 0 \end{pmatrix} , \tag{A.24}
$$

where $A^{(\prime)}$ and $B^{(\prime)}$ have been defined in Table VIII. Without k_{3T}, the conjugate variable b_2 in the Sudakov exponent $S_\pi(t)$ is set to b_1.

---

[1] Heavy Flavor Averaging Group, hep-ex/0505100; updated in http://www.slac.stanford.edu/xorg/hfag.
[2] Y.Y. Keum, H-n. Li, and A.I. Sanda, Phys Lett. B **504**, 6 (2001); Phys. Rev. D **63**, 054008 (2001).
[3] C.D. Lü, K. Ukai, and M.Z. Yang, Phys. Rev. D **63**, 074009 (2001).
[4] L.L. Chau, H.Y. Cheng, and B. Tseng, Phys. Rev. D **43**, 2176 (1991).
[5] M. Gronau, O.F. Hernández, D. London, and J.L. Rosner, Phys. Rev. D **50** 4529, (1994); Phys. Rev. D **52** 6356, (1995); Phys. Rev. D **52** 6374, (1995).
[6] Y.Y. Charng and H-n. Li, Phys. Lett. B. **594**, 185 (2004).
[7] T. Yoshikawa, Phys. Rev. D **68**, 054023 (2003); S. Mishima and T. Yoshikawa, Phys. Rev. D **70**, 094024 (2004).
[8] M. Kobayashi and T. Maskawa, Prog. Th. Phys. **49**, 652 (1973).
[9] A.J. Buras, R. Fleischer, S. Recksiegel, and F. Schwab, Phys. Rev. Lett. **92**, 101804 (2004); Nucl.Phys. **B697**, 133 (2004).
[10] S. Nandi and A. Kundu, hep-ph/0407061.
[11] M. Gronau and J.L. Rosner, Phys. Lett. B **572**, 43 (2003).
[12] M. Ciuchini et al., hep-ph/0407073.
[13] Y.Y. Charng and H-n. Li, Phys. Rev. D **71**, 014036 (2005).
[14] X.G. He and B. McKellar, hep-ph/0410098.
[15] C.W. Chiang, M. Gronau, J.L. Rosner, and D.A. Suprun Phys. Rev. D **70**, 034020 (2004).
[16] Z. Ligeti, Int. J. Mod. Phys. A **20**, 5105 (2005).
[17] Y.L. Wu and Y.F. Zhou, Phys. Rev. D **71**, 021701 (2005).
[18] S. Baek, P. Hamel, D. London, A. Datta, and D.A. Suprun, Phys. Rev. D **71**, 057502 (2005).
[19] S.J. Brodsky, G.P. Lepage, and P.B. Mackenzie, Phys. Rev. D **28**, 228 (1983).
[20] H-n. Li and G. Sterman, Nucl. Phys. **B381**, 129 (1992).
[21] T. Kurimoto, H-n. Li, and A.I. Sanda, Phys. Rev. D **65**, 014007 (2002).
[22] C.H. Chen, Y.Y. Keum, and H-n. Li, Phys. Rev. D **64**, 112002 (2001); Phys. Rev. D **66**, 054013 (2002).
[23] S. Mishima, Phys. Lett. B **521**, 252 (2001).
[24] Y.Y. Keum and A. I. Sanda, Phys. Rev. D **67**, 054009 (2003).
[25] M. Beneke, G. Buchalla, M. Neubert and C.T. Sachrajda, Phys. Rev. Lett. **83**, 1914 (1999); Nucl. Phys. **B591**, 313 (2000); Nucl. Phys. **B606**, 245 (2001).
[26] C.H. Chen and H.N. Li, Phys. Rev. D **63**, 014003 (2001).
[27] Y. Li and C.D. Lü, hep-ph/0508032.
[28] C.H. Chen, in preparation.
[29] H.Y. Cheng, C.K. Chua, and A. Soni, Phys. Rev. D **71**, 014030 (2005).
[30] C.W. Bauer, D. Pirjol, I.Z. Rothstein, and I.W. Stewart, Phys. Rev. D **70**, 054015 (2004).
[31] G. Buchalla, A. J. Buras, and M. E. Lautenbacher, Review of Modern Physics, **68**, 1125 (1996).
[32] V.L. Chernyak and A.R. Zhitnitsky, Phys. Rept. **112**, 173 (1984).
[33] M. Beneke and M. Neubert, Nucl. Phys. **B675**, 333 (2003).
[34] M. Neubert, talk presented at CKM 2005, San Diego, Mar. 15-18, 2005.
[35] D.s. Du, J.f. Sun, D.s. Yang, and G.h. Zhu, Phys. Rev. D **67**, 014023 (2003).
[36] R. Aleksan, P. F. Giraud, V. Morenas, O. Pene, and A. S. Safir, Phys. Rev. D **67**, 094019 (2003).
[37] H.Y. Cheng, C.K. Chua, and A. Soni, Phys. Rev. D **72**, 014006 (2005).
[38] M. Beneke, Phys. Lett. B **620**, 143 (2005).
[39] C.H. Chang and H-n. Li, Phys. Rev. D **55**, 5577 (1997).
[40] Y.Y. Keum and H-n. Li, Phys. Rev. **D63**, 074006 (2001).
[41] H-n. Li and H.L. Yu, Phys. Rev. Lett. **74**, 4388 (1995); Phys. Lett. B **353**, 301 (1995); Phys. Rev. D **53**, 2480 (1996).
[42] T.W. Yeh and H-n. Li, Phys. Rev. D **56**, 1615 (1997).
[43] H.Y. Cheng and K.C. Yang, Phys. Rev. D **63**, 074011 (2001).
[44] A. Ali, E. Lunghi, and A. Parkhomenko, Eur. Phys. J. C **36**, 183 (2004).
[45] C.N. Burrell and A.R. Williamson, hep-ph/0504024.
[46] X. Li and Y. Yang, Phys. Rev. D **72**, 074007 (2005).
[47] C.W. Bauer, I.Z. Rothstein, and I.W. Stewart, hep-ph/0510241.
[48] M. Bauer and M. Wirbel, Z. Phys. **C42**, 671 (1989).
[49] H-n. Li and H.S. Liao, Phys. Rev. D **70**, 074030 (2004).
[50] T. Huang, C.F. Qiao, and X.G. Wu, hep-ph/0507270.

[51] H. Kawamura, J. Kodaira, C.F. Qiao, and K. Tanaka, Phys. Lett. B **523**, 111 (2001); Mod. Phys. Lett. A **18**, 799 (2003).
[52] Z.T. Wei and M.Z. Yang, Nucl. Phys. **B642**, 263 (2002); C.D. Lu and M.Z. Yang, Eur. Phys. J. C **28**, 515 (2003).
[53] V.M. Braun and I.E. Filyanov, Z Phys. C **48**, 239 (1990); P. Ball, J. High Energy Phys. **01**, 010 (1999).
[54] T. Huang and X.G. Wu, Phys. Rev. D **71**, 034018 (2005).
[55] H-n. Li, Prog. Part. Nucl. Phys. **51**, 85 (2003); Czech. J. Phys. **53**, 657 (2003).
[56] A. Khodjamirian and R. Ruckl, Phys. Rev. D **58**, 054013 (1998).
[57] P. Ball J. High Energy Phys. **09**, 005 (1998); Z. Phys. C **29**, 637 (1985).
[58] P. Ball and R. Zwicky, Phys. Rev. D **71**, 014015 (2005).
[59] HPQCD Collaboration, A. Gray et al., hep-lat/0507015.
[60] CLEO Collaboration, S.B. Athar et al., Phys. Rev. D **68**, 072003 (2003).
[61] Particle Data Group Collaboration, S. Eidelman *et al.*, Phys. Lett. B **592**, 1 (2004).
[62] Z. Luo and J.L. Rosner, Phys. Rev. D **68**, 074010(2003).
[63] V.M. Braun and A. Lenz, Phys. Rev. D **70**, 074020 (2004).
[64] A. Khodjamirian, Th. Mannel, and M. Melcher, Phys. Rev. D **70**, 094002 (2004).
[65] K. Abe, talk presented at XXII International Symposium on Lepton-Photon Interactions at High Energy, Jun. 30-Jul. 5, 2005, Uppsala, Sweden.
[66] J. Smith, talk presented at CKM 2005, San Diego, Mar. 15-18, 2005.
[67] T. Huang, M.Z. Zhou, and X.H. Wu, Eur. Phys. J. C **42**, 271 (2005).
[68] W.S. Hou, M. Nagashima, and A. Soddu, Phys. Rev. Lett. **95**, 141601 (2005).
[69] V. Barger, C.W. Chiang, P. Langacker, and H.S. Lee Phys. Lett. B **598**, 218 (2004).
[70] M. Beneke and D. Yang, hep-ph/0508250.
[71] J.C. Collins and D.E. Soper, Nucl. Phys. **B193**, 381 (1981).
[72] J. Botts and G. Sterman, Nucl. Phys. **B325**, 62 (1989).
[73] H-n. Li, Phys. Rev. D **66**, 094010 (2002); K. Ukai and H-n. Li, Phys. Lett. B **555**, 197 (2003).
[74] S. Mishima and A.I. Sanda, Prog. Theor. Phys. **110**, 549 (2003).
[75] C.H. Chen and H-n. Li, Phys. Rev. D **71**, 114008 (2005).